Naval Research Laboratory
Washington, DC 20375-5320

Applying the Delay-Curve Hough Transform To Shallow-Water Environments

Haw-Jye Shyu
Wendell L. Anderson

Advanced Information Technology
Information Technology Division

September 9, 1998

REPORT DOCUMENTATION PAGE

Public reporting burden for this collection of information is estimated to average 1 hour per response, including the time for reviewing instructions, searching existing data sources, gathering and maintaining the data needed, and completing and reviewing the collection of information. Send comments regarding this burden estimate or any other aspect of this collection of information, including suggestions for reducing this burden, to Washington Headquarters Services, Directorate for Information Operations and Reports, 1215 Jefferson Davis Highway, Suite 1204, Arlington, VA 22202-4302, and to the Office of Management and Budget, Paperwork Reduction Project (0704-0188), Washington, DC 20503.

1. AGENCY USE ONLY (*Leave Blank*)	2. REPORT DATE	3. REPORT TYPE AND DATES COVERED
	September 9, 1998	

4. TITLE AND SUBTITLE	5. FUNDING NUMBERS
Applying the Delay-Curve Hough Transform to Shallow-Water Environments	ONR - UW-14-2-04 PE - 62314N

6. AUTHOR(S)

Haw-Jye Shyu and Wendell L. Anderson

7. PERFORMING ORGANIZATION NAME(S) AND ADDRESS(ES)	8. PERFORMING ORGANIZATION REPORT NUMBER
Naval Research Laboratory Washington, DC 20375-5320	NRL/FR/5580--98-9888

9. SPONSORING/MONITORING AGENCY NAME(S) AND ADDRESS(ES)	10. SPONSORING/MONITORING AGENCY REPORT NUMBER
Office of Naval Research 800 North Quincy Street Arlington, VA 22217-5660	

11. SUPPLEMENTARY NOTES

12a. DISTRIBUTION/AVAILABILITY STATEMENT	12b. DISTRIBUTION CODE
Approved for public release; distribution is unlimited.	

13. ABSTRACT (*Maximum 200 words*)

The Delay-Curve Hough Transform (DCHT) has been proposed to detect the correlation traces produced by constant velocity targets in broadband correlograms and to estimate target track parameters. The derivation of the DCHT assumed that the sound velocity profile (SVP) is a constant and the correlation trace is due to the direct propagation path. These assumptions are not true in the shallow-water environments. This study investigates the use of the DCHT in these environments by examining the effects of the SVP on the correlation traces appearing in broadband correlograms for three different shallow-water environments. The GAMARAY model, an eigenray-based sound propagation model, was used to produce the sound field. Even though beyond some short ranges the direct propagation path disappears and the dominant eigenrays are due to multipath, the correlation traces still maintain the shape of the analytic delay curves, and the DCHT successfully detects the targets. The estimates of target heading, speed factor, and closest point of approach (CPA) time by the DCHT proved to be accurate. However, in most cases, estimates of the depth factor were incorrect. A theoretical explanation for the unreliability of the estimation of the depth factor is also given.

14. SUBJECT TERMS		15. NUMBER OF PAGES
Hough transform Cross-correlation Correlogram	Shallow-water environments Eigenrary model	38
		16. PRICE CODE

17. SECURITY CLASSIFICATION OF REPORT	18. SECURITY CLASSIFICATION OF THIS PAGE	19. SECURITY CLASSIFICATION OF ABSTRACT	20. LIMITATION OF ABSTRACT
UNCLASSIFIED	UNCLASSIFIED	UNCLASSIFIED	UL

CONTENTS

APPLYING THE DELAY-CURVE HOUGH TRANSFORM
TO SHALLOW-WATER ENVIRONMENTS

1. INTRODUCTION

The broadband correlogram, a two-dimensional display over time of the cross-correlation received by a two-sensor system, has proven to be a useful tool in the detection and tracking of targets moving in the ocean. The two-sensor system can be two omnidirectional hydrophones, two halves of a split-array, or two separate neighboring sensor arrays. The correlogram is a historical record of the cross-correlation between the signals received at the two sensors. When detected by the two sensors, a target traveling with constant speed and heading (i.e., course) generates a trace in the correlogram produced by the system. Because the location of the trace is a measure of the relative time delay of the signal arriving at the two sensors, the trace is often referred to as a *delay curve*. Figure 1 shows a typical broadband correlogram. The vertical axis of the correlogram is the observation time, while the horizontal axis is the time difference of arrival of the signal at the two sensors. The intensity of the correlogram at a point is a measure of the correlation between the two received signals. As can be seen in this figure, many dark traces (delay curves) are visible in the correlogram. A dark trace with a small slope indicates that the corresponding acoustic source is either very close to the sensor array or is moving relatively fast. On the other hand, a dark trace with a large slope indicates the corresponding acoustic source is either far away from the sensor array or is moving relatively slowly.

Assuming that the sound velocity profile (SVP) is constant and independent of geographic location, that the sound wave propagation from the target to the sensors is a straight-line path, and that a target is traveling with constant speed, heading, and depth, then the resulting 'ideal' delay curve of the target was shown [1] to be a member of a family of analytic equations. The analytic equation of the delay curve is defined by the target track parameters: speed (v), heading (θ), target horizontal range (D) at the closest point of approach (CPA), time of CPA (t_0), and the relative depth (h) of the source with respect to the sensor. That report proposed the Delay-Curve Hough Transform (DCHT), a modified Hough Transform, as an automated method for detecting delay curves and estimating the parameters of the corresponding track. The essence of the DCHT is to hypothesize a family of potential delay curves, accumulate evidence for each potential delay curve by summing all the pixel values along the curve and normalizing the accumulated value by the total number of pixels in the summing process, and threshold the normalized pixel values in the parameter space to detect a peak. The parameters of the target track can be estimated from the location of the peak in the parameter space. Assuming white noise, the normalized integration process can theoretically provide 5 log(N) dB processing gain, where N is the number of cross-correlation values involved in the integration process of the DCHT.

Two sets of assumptions were used in the development of the DCHT: first, the sound propagation was a straight line between the source and the receiver, and second, the target traveled with constant speed, heading, and depth during the integration interval of the DCHT. These assumptions proved to be good for the original application of the DCHT to long-range deep-water surveillance scenarios. However, as this technique is applied to littoral areas, the first assumption may no longer hold. A shallow-water environment is distinctly different from that of deep-water environment; in a shallow-water environment, the SVP is more
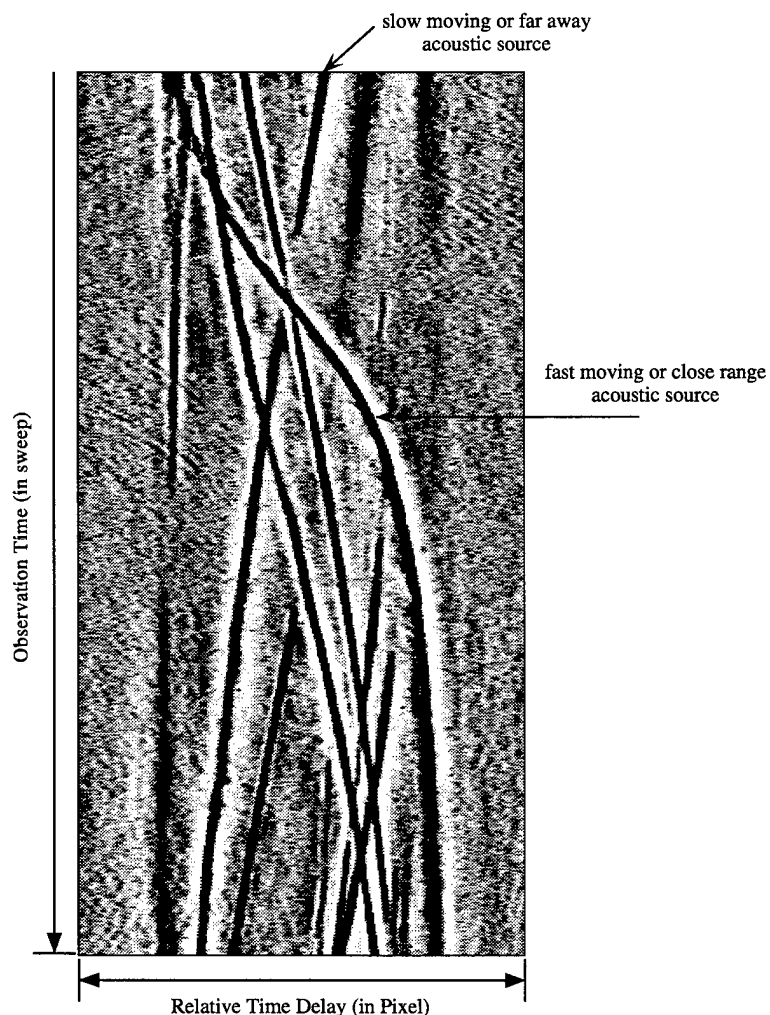
Fig. 1 — A typical split-array beamformed broadband correlogram

complex, and interactions of the propagated signal with the surface and the bottom lead to complicated multipath propagation. This report examines the applicability of the DCHT in shallow-water environments by examining the effect of the SVP on the correlation traces of a constant velocity target. Degradation due to the variation in the course and speed of the target were not part of this study.

To understand the behavior of a delay curve in a shallow-water environment, three different, real, shallow-water SVPs were studied. The GAMARAY model [2], a ray-based broadband acoustic propagation model developed at the Applied Research Laboratory, University of Texas at Austin, was used to generate acoustic fields based on these SVPs. Using an algorithm [3] developed by Fred Machell of the Applied Research Laboratory, University of Texas at Austin, broadband correlograms were then produced from these fields and the DCHT was applied to these correlograms.

The rest of this report is organized as follows. Section 2 discusses the analytic equations associated with the DCHT. Section 3 presents the three different shallow-water environments and a set of target scenarios. Based on the scenarios presented in Section 3, Section 4 shows the delay curves generated by the mathematical model (the analytic equation of the delay curve), while Section 5 presents the broadband correlograms generated with acoustic data produced by the GAMARAY model for each SVP. Section 6 shows the detection results of the DCHT. Section 7 presents an analysis on the depth effect. Section 8 presents the conclusions.

2. THEORETICAL CONSIDERATIONS

The Time-Delay Curve

As a target moves by a two-sensor system, the time difference of arrival of the received signals is given by a time-delay curve. Figure 2 shows the relative geometry between the target and the two sensors. The target is moving with a constant speed (v), heading (θ), and relative depth (h) to the sensors. The two sensors are assumed to be at the same depth. The target reaches its CPA to the center of the sensor pair (L and R) at location ($x0$, $y0$, h) and at time t_0. At this time the target is at a horizontal distance (D) from the center of the sensor pair. Assuming a plane wavefront arrival at the two sensors, Stevens and Shyu [1] showed that the equation of the delay curve is:

$$\tau(t) = \tau_{max} \frac{\left(\frac{v}{D}(t - t_0)\right)\cos\theta - \sin\theta}{\sqrt{1 + \left(\frac{v}{D}(t - t_0)\right)^2 + \left(\frac{h}{D}\right)^2}} , \tag{1}$$

where:

D is horizontal distance at CPA from the target to the sensors' midpoint,

h is depth difference between the target and the sensors,

v is target speed,

θ is target heading,

t is the observation time,

t_0 is CPA time,

$\tau(t)$ is relative time delay between the two received signals at time t, and

τ_{max} is distance between the two sensors divided by the speed of sound.

Further details of the delay curve (such as the effect of v/D and h/D on the shape of the delay curve, the point spread function of the DCHT, etc.) are given in a previous report [1].

The Broadband Correlation Function

The broadband cross-correlation function over a time interval T of a source signal arriving at two different sensors is given by the equation

$$F(t, \tau) = \frac{\int_{-T/2}^{T/2} b_1(x+t+\tau)b_2(x + t)dx}{\sqrt{\int_{-T/2}^{T/2}|b_1(x+t+\tau)|^2\,dx}\,\sqrt{\int_{-T/2}^{T/2}|b_1(x+t)|^2\,dx}} , \tag{2}$$

where

T is integration time,

t is center of the integration time interval,

τ is assumed time difference in arrival of the signal at the two sensors,

$b_1(y)$ is band-limited signal received at time y for sensor 1,

$b_2(y)$ is band-limited signal received at time y for sensor 2, and

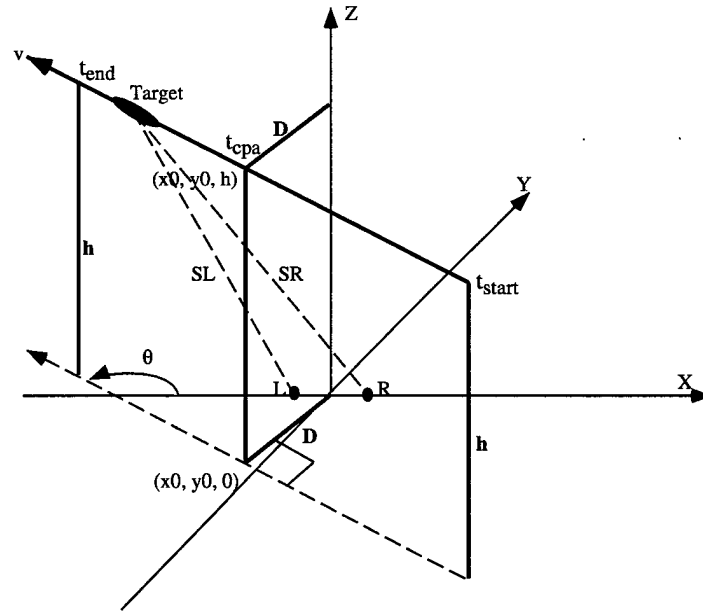$F(t,\tau)$ is cross-correlation value at time t for the time-delay difference τ.

Fig. 2 — Target-sensor geometry. *L* and *R* are the location of the two
channels (or the centers of the two subarrays). The closest point of ap-
proach (CPA) is denoted as (*x0*, *y0*, *h*). The horizontal distance of the
signal source at the CPA is denoted as *D*. The relative depth difference
between the target and the sensor is denoted as *h*. The track direction of
the signal source is θ, which is measured from positive *X*-axis on the *XY*-
plane. *SL* and *SR* are the distance from the target to sensor *L* and *R*, re-
spectively. The target speed is *v*. Here t_{start}, t_{end}, and t_{cpa} indicate the be-
ginning of observation, the ending of observation, and the CPA time, re-
spectively.

For band-limited white noise and nondispersive propagation, the cross-correlation function is a cosine
function modulated by a sinc function

$$F(\tau) = \left[\frac{\sin(\pi B(\tau - \tau_0))}{\pi B(\tau - \tau_0)}\right]\cos(2\pi f_0(\tau - \tau_0)) ,$$

where τ_0 is the time difference of arrival between the signals received at the two sensors. $F(\tau)$ is defined by
the center frequency (f_0) and the bandwidth (B) of the noise. The width of the sinc function is inversely
proportional to B, while the width of the cosine function is inversely proportional to f_0. For the nondispersive
propagation problem, where the wave propagation speed is independent of the frequency, the peak of the
sinc function occurs at the same delay time as a peak of the cosine function. For the dispersive propagation
problem, where the wave propagation speed is a function of frequency (such as a shallow-water environ-
ment), the behavior of the cross-correlation function is more complicated. The peak of the sinc function and
the peak of the cosine function do not coincide. In fact, the peak of the sinc function occurs at a time delay
inversely proportional to the group velocity of the sound wave, while the peaks of the cosine function occur
at time delays inversely proportional to the phase velocity of the sound wave. Reference 5 further discusses
the behavior of the cross-correlation function.

The Delay-Curve Hough Transform

The Delay-Curve Hough Transform (DCHT) detects delay curves by performing integration along the trajectories of possible delay curves in the correlogram, normalizing the integrated pixel values by the total number of pixels involved in the integration process, storing the normalized pixel value in the parameter space, and thresholding these values. A peak exceeding the threshold indicates the detection of a delay curve, and the location of the peak in the parameter space defines the corresponding track parameters. For a given sensor pair, the integration and normalization process can be mathematically denoted as

$$f\left(\frac{v}{D}, \theta, t_0, \frac{h}{D}\right) = \frac{1}{N} \iint F(x, y) \delta(t(x, y)) \, dx \, dy, \tag{3}$$

where

$f(v/D, \theta, t_0, h/D)$	is the output of the DCHT,
$\delta(t)$	is the Dirac-delta function restricting the integration to the delay curve,
N	is the total number of pixels in the integration,
$F(x,y)$	is the pixel value in the correlogram at location (x,y),
x	is the horizontal offset, and
y	is the vertical offset.

The time-delay curve is a function of the five parameters v, θ, h, D, and t_0. Since v, h, and D appear only as the ratios v/D and h/D, the parameter space of the DCHT has only four dimensions: θ, t_0, v/D, and h/D. Each dimension is independently sampled over an appropriate range for the tracks of interest.

3. REAL-WORLD SCENARIOS

The time-delay curve equation was developed assuming that the speed of sound was constant over the field and that the propagation of the signal from the source to each of the sensors was along a direct straight line path. In the real world, especially in shallow-water environments, the situation is much more complex. Since the SVP is actually a function of depth, the sound wave propagation is no longer a straight line but a set of different multiple paths.

Sound velocity profiles from three different locations were used to study the effects on the DCHT of the propagation in a shallow-water environment. These sound velocity profiles are identified as SVP I, SVP II, and SVP III and are shown in Fig. 3. For SVP I, the depth of the water is about 250 m; the sound speed decreases monotonically from 1536 m/s at the surface to 1513 m/s at a depth of 100 m and then remains nearly constant from 100 m to the bottom. For SVP II, the water depth is 65 m; the sound speed decreases monotonically from 1545 m/s at the surface to 1512 m/s at the bottom, with the sound speed nearly constant from the surface to a depth of 10 m and from a depth of 40 m to a depth of 50 m. For SVP III, the sound speed is nearly constant at 1505 m/s from the surface to a depth of 25 m, rapidly decreases to a speed of 1455 m/s at a depth of 45 m, and increases slowly from the 45 m depth to the bottom. The sea bottom is assumed to be flat and has one layer. Table 1 gives the geoacoustic parameters, where CP is the compressional velocity of the sound wave, CS is the shear velocity of the sound wave, RHO is the density of the sediment, KP is the compressional wave attenuation, and KS is the shear wave attenuation. Here, 1 indicates the values for the top of the layer and 2 indicates the values for the bottom of the layer.

(a) Sound Velocity Profile I   (b) Sound Velocity Profile II   (c) Sound Velocity Profile III
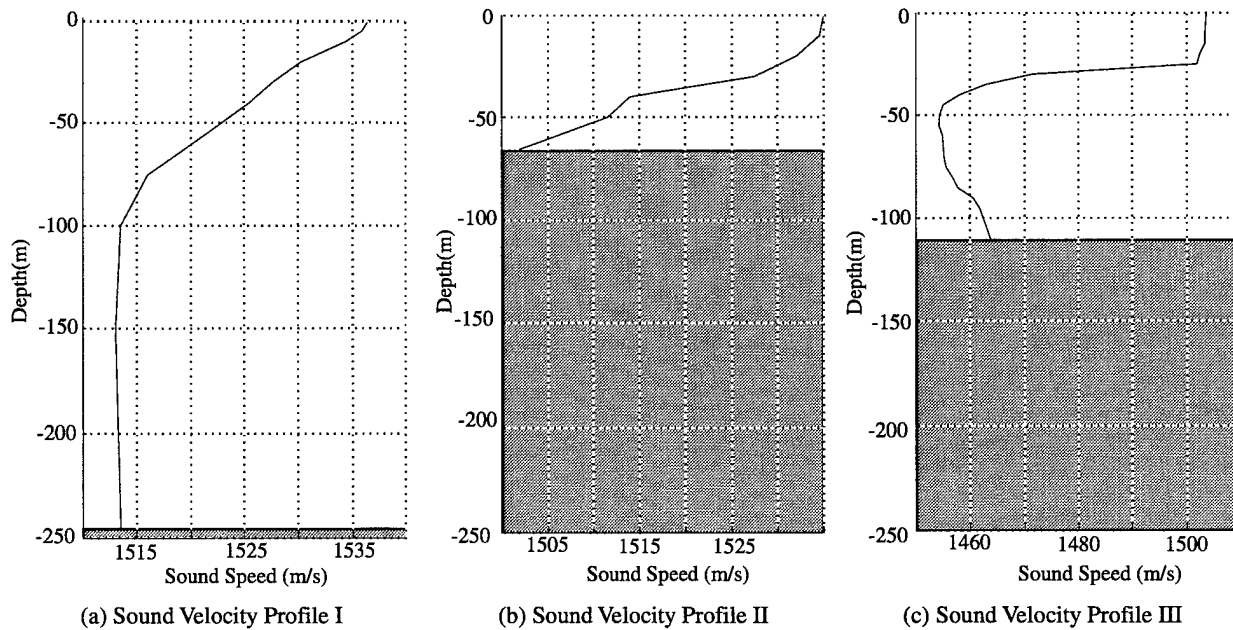
Fig. 3 — Three different shallow-water sound velocity profiles. Sea bottom is shown as the shaded area.

Table 1 — The Geoacoustic Parameters of Sea Bottom

	SVP I	SVP II	SVP III
Thickness (m)	175	2500	2500
CP1 (m/s)	1572	1485	1485
CP2 (m/s)	1782	2600	2600
CS1 (m/s)	263	35	35
CS2 (m/s)	425	1066	1066
RHO1 (g/cc)	1.56	1.61	1.61
RHO2 (g/cc)	1.81	2.40	2.40
KP1(dB/m-kHz)	0.04	0.08	0.08
KP2(dB/m-kHz)	0.08	0.03	0.03
KS1(dB/m-kHz)	4	13	13
KS2(dB/m-kHz)	4	8	8

4. DELAY CURVES GENERATED BY THE ANALYTIC EQUATION

Figure 4 shows that two hydrophones were used for the GAMARAY model simulation with target-sensor geometries. The distance between the two bottom-mounted sensors is 100 m. Four target courses ($0°$, $30°$, $60°$, and $270°$) and five different CPA distances (0.1 km, 0.25 km, 0.5 km, 1.0 km, and 2.0 km) were used in this study. In each case, the target traveled at a constant speed (4.32 knots) over a distance of 4 km for 30 min with the target reaching CPA at the middle of the run. Target depth was 40 m. Using the analytic equation, a constant sound speed is needed to generate the delay curves. The median sound speed of the SVP was used in generating the delay curves shown in this section. Since the different SVPs have different water depths, the value of h/D for a given CPA range will be different for each SVP. Table 2 shows the values of h/D. The values of v/D are independent of the SVP and are given in Table 3.

(a) Target course at 0°

(b) Target course at 30°

(c) Target course at 60°
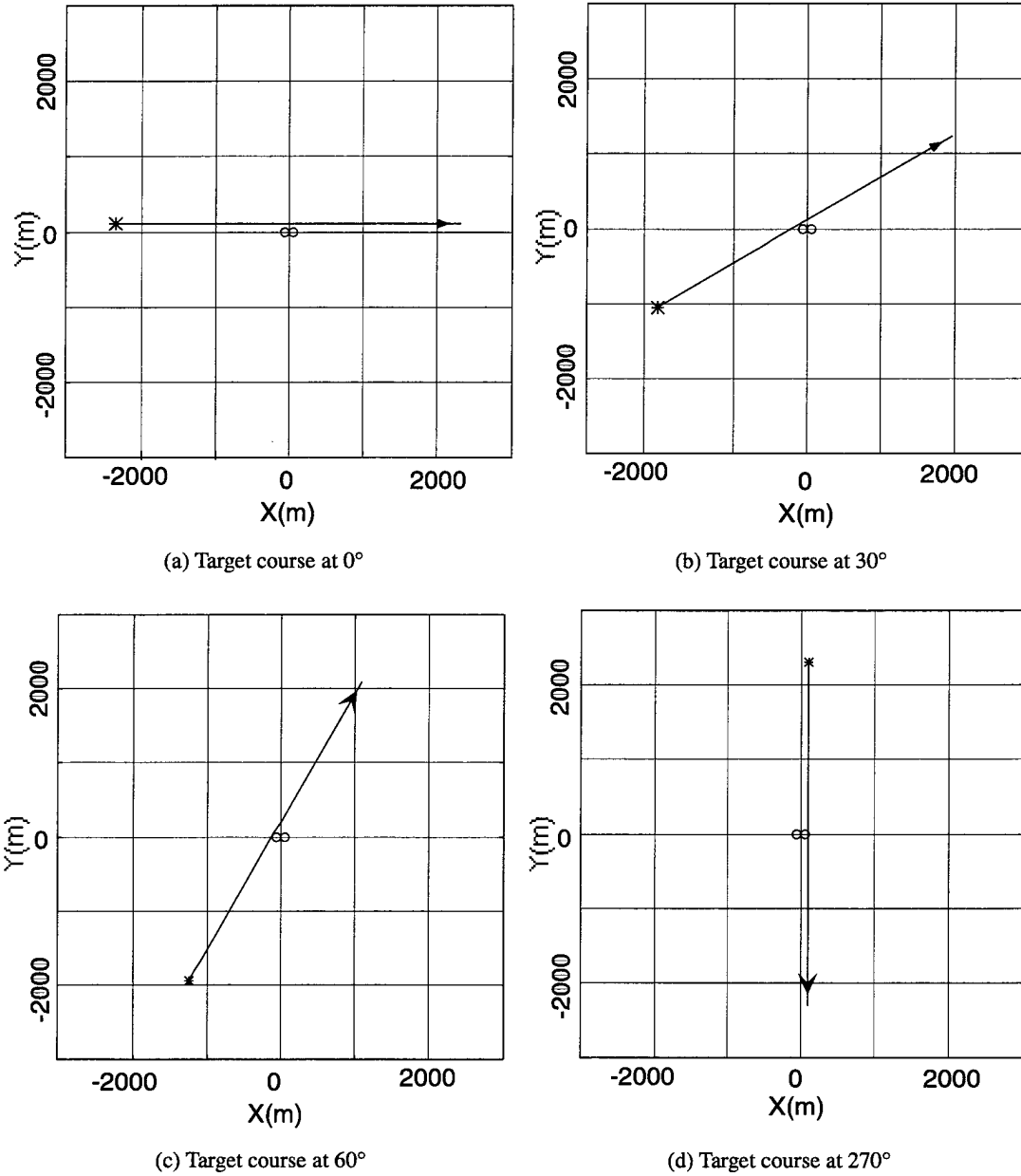

(d) Target course at 270°

Fig. 4 — Target-sensor geometry. The locations of the two phase centers are indicated by the two neighboring circles. The star (*) indicates the initial position of the target. The observation time is about 30 min with the CPA in the middle of the run. The speed of the target is about 4.32 knots. The CPA distance shown is 100 m; CPA distances of 0.1, 0.25, 0.5, and 1.0 km were also used in this study. The target depth is 40 m.

Table 2 — h/D Values for Each SVP at Different CPA Ranges (D)

	$D = 0.1$ km	$D = 0.25$ km	$D = 0.5$ km	$D = 1.0$ km	$D = 2.0$ km
SVP I	2.05	0.82	0.41	0.205	0.1025
SVP II	0.25	0.1	0.05	0.025	0.0125
SVP III	0.7	0.28	0.14	0.07	0.035

Table 3 — v/D Value at Different CPA Ranges (D)

	$D = 0.1$ km	$D = 0.25$ km	$D = 0.5$ km	$D = 1.0$ km	$D = 2.0$ km
v/D	0.3125	0.125	0.0625	0.03125	0.015625

Figure 5(a) shows the delay curves for each of the three SVPs for the five different CPA ranges for a target heading of 0°. For each CPA range, there is a delay curve for each SVP; the delay curve for SVP I is the lightest trace, the delay curve for SVP II is the intermediate trace, and the delay curve for SVP III is the darkest trace. Likewise, Figs. 5(b), 5(c), and 5(d) show the delay curves for the five different CPA ranges for target headings of 30°, 60°, and 270°, respectively. Note that the delay curve for a target heading of 270° is equivalent to that of a 90° with the exception that the peak of the delay-curve points to the right instead of the left. These four headings were chosen to provide a rough sampling of delay-curve behaviors.

For CPA distances greater than 1.0 km, observed from Figs. 5(a) through 5(d), the differences among the delay curves for the three SVPs are negligible. At the distance of 0.5 km, small differences can be seen for target headings of 60° and 270°. For target CPA ranges shorter than 0.25 km, significant differences in the delay curves are apparent when the target is near CPA. This is the horizontal compression/expansion effect due to the variation of h/D [1]. The larger the h/D, the larger the compression of the delay curve. For a given target depth and CPA range, the deeper the ocean the greater the value of h/D. Since SVP I is the deepest, it will have the most compression. Furthermore, this horizontal compression/expansion effect is especially significant for a target heading at 270° (or 90°) when the target is near the CPA. From Eq. (1), near CPA (when t is approximately equal to t_0), the absolute value of the numerator is a constant (τ_{max}) and the denominator will be dominated by the h/D ratio, resulting in a significant horizontal compression.

As the target CPA range increases, the shape of the delay-curve approaches a straight line. This vertical expansion effect is due to the change in the v/D ratio [1]; the smaller the value of v/D, the larger the vertical expansion of the delay curve. For a given target speed, a larger target CPA range (D) results in a smaller value of the v/D ratio and, hence, a more straightened delay curve.

Since these delay curves were generated by the analytic equation based on sensor-target geometry, they are referred to as the geometrically modeled delay curves. The DCHT uses these geometrically modeled delay curves as templates for its integration process. If the geometrically modeled delay curve does not match with the correlation trace, then the normalized integrated value will be degraded. On the other hand, if the geometrically modeled delay curve matches the correlation trace, then the normalized integrated value will be enhanced. The detection by the DCHT is thus dependent on how well the geometrically modeled delay curve matches the real correlation trace in the correlograms.

(i) — CPA range = 0.1 km

(ii) — CPA range = 0.25 km

(iii) — CPA range = 0.5 km

(iv) — CPA range = 1.0 km
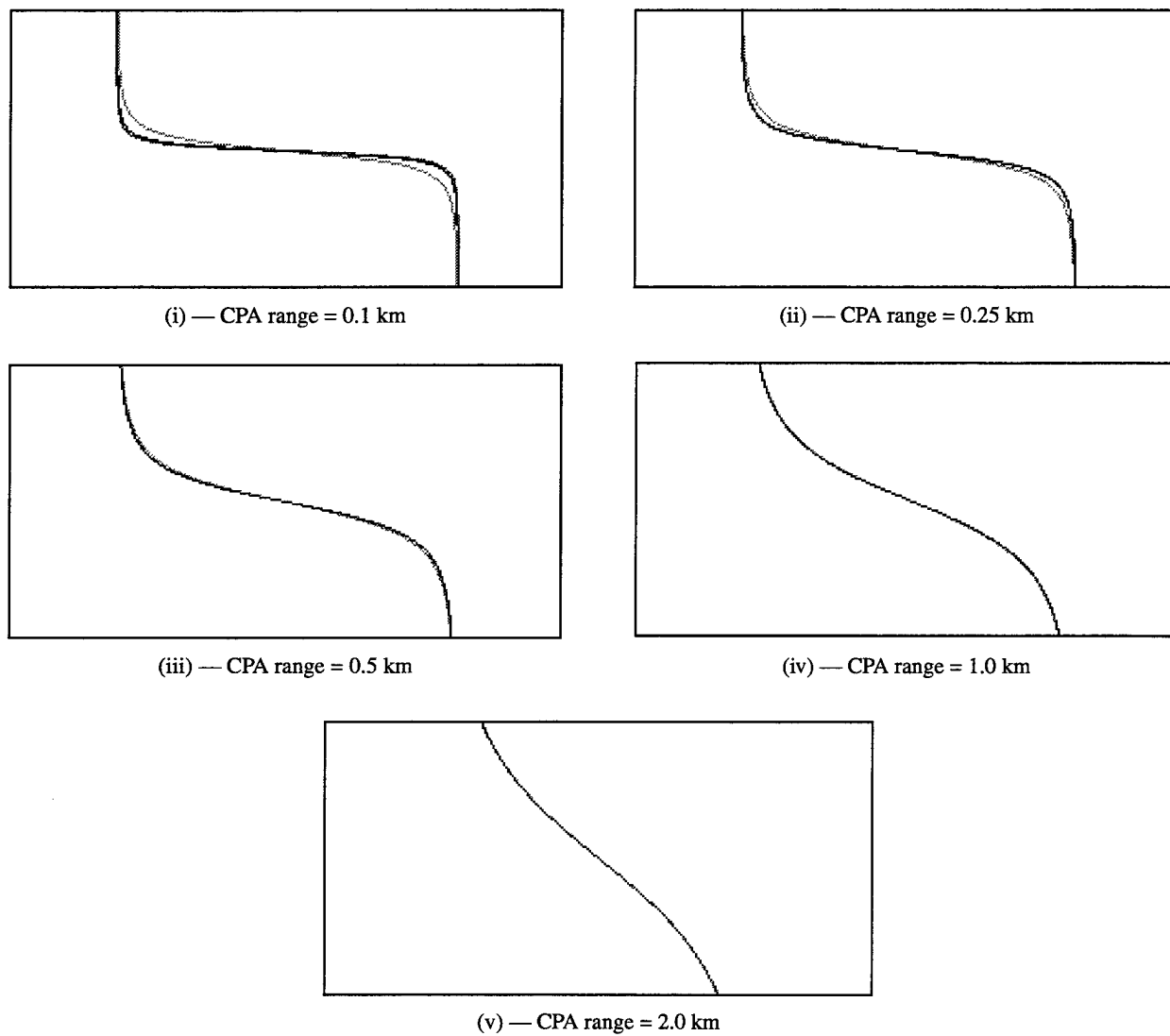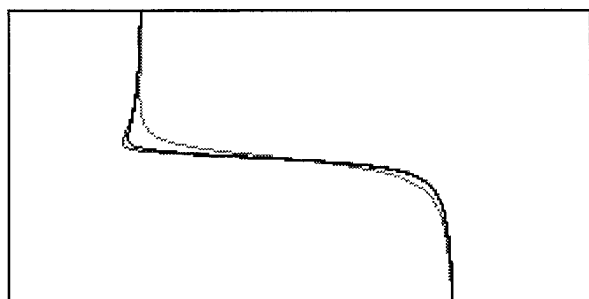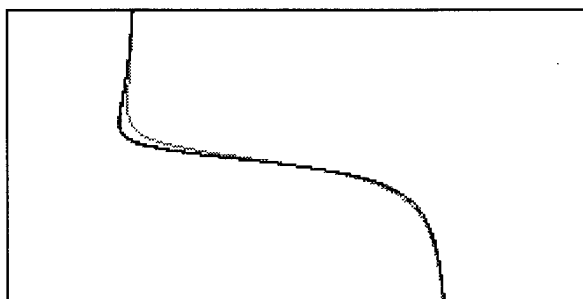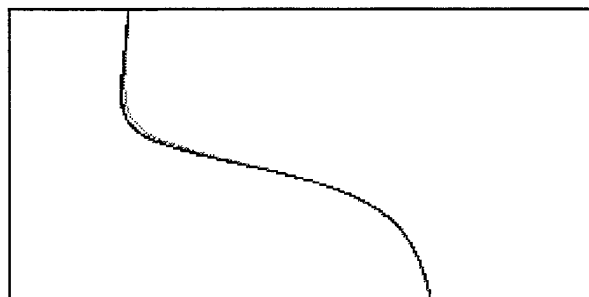
(v) — CPA range = 2.0 km

Fig. 5(a) — Delay curves generated by the analytic equation using the track parameters specified in Fig. 4(a) with heading = 0°; SVP I is the lightest, SVP II is the intermediate, and SVP III is the darkest.
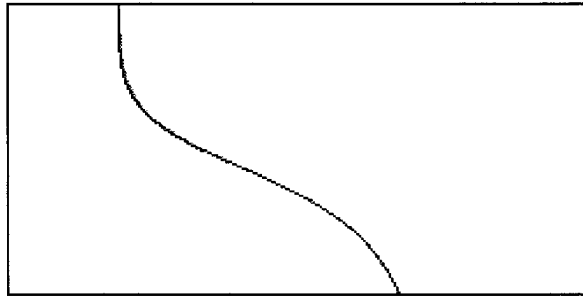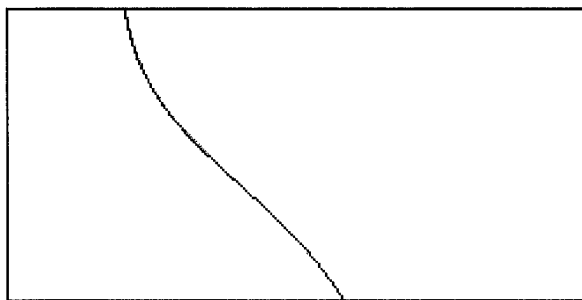
(i) — CPA range = 0.1 km

(ii) — CPA range = 0.25 km

(iii) — CPA range = 0.5 km

(iv) — CPA range = 1.0 km

(v) — CPA range = 2.0 km

Fig. 5(b) — Delay curves generated by the analytic equation using the track parameters specified in Fig. 4(b) with heading = 30°; SVP I is the lightest, SVP II is the intermediate, and SVP III is the darkest.
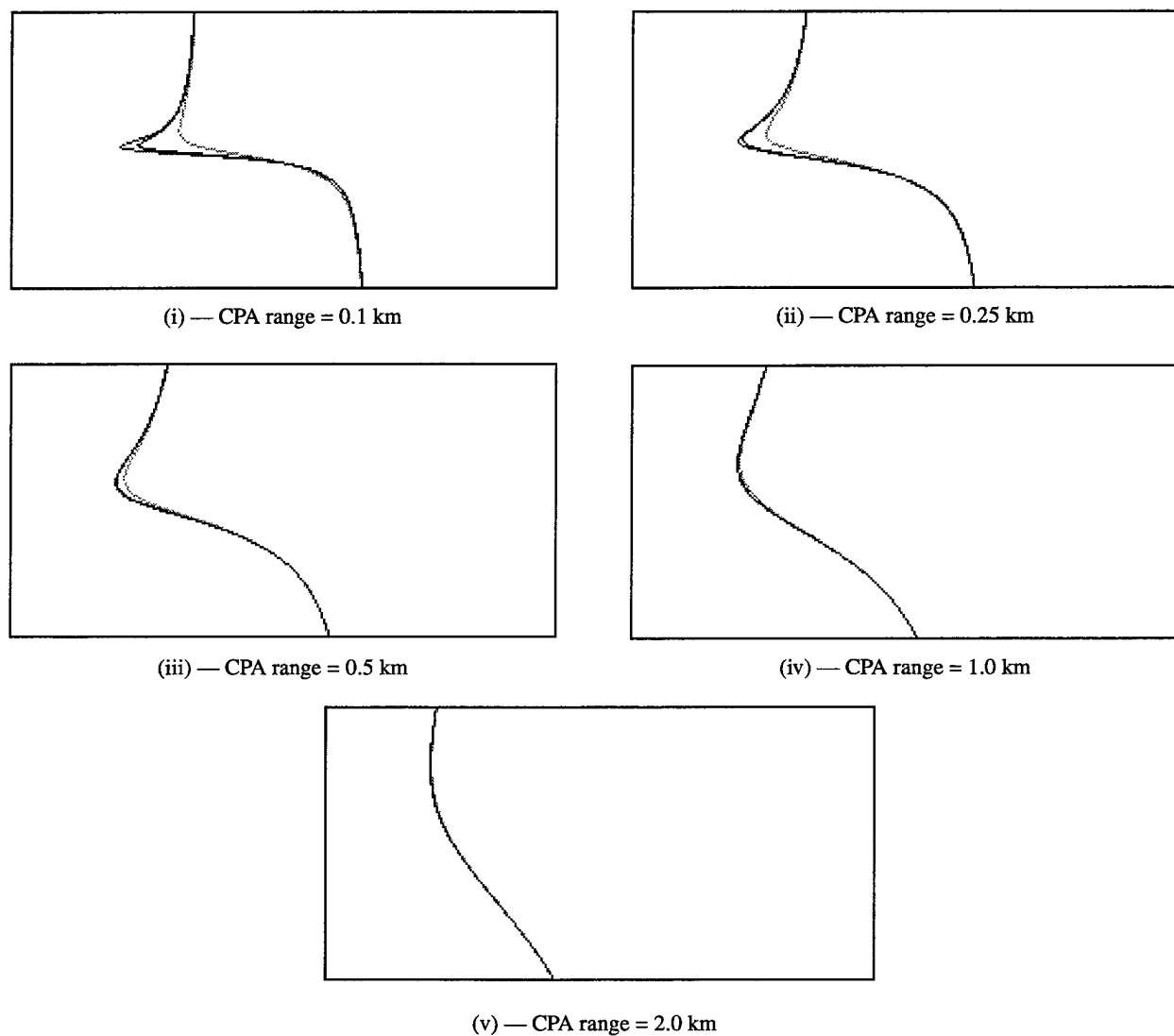
(i) — CPA range = 0.1 km

(ii) — CPA range = 0.25 km

(iii) — CPA range = 0.5 km

(iv) — CPA range = 1.0 km

(v) — CPA range = 2.0 km

Fig. 5(c) — Delay curves generated by the analytic equation using the track parameters specified in Fig. 4(c) with heading = 60°; SVP I is the lightest, SVP II is the intermediate, and SVP III is the darkest.
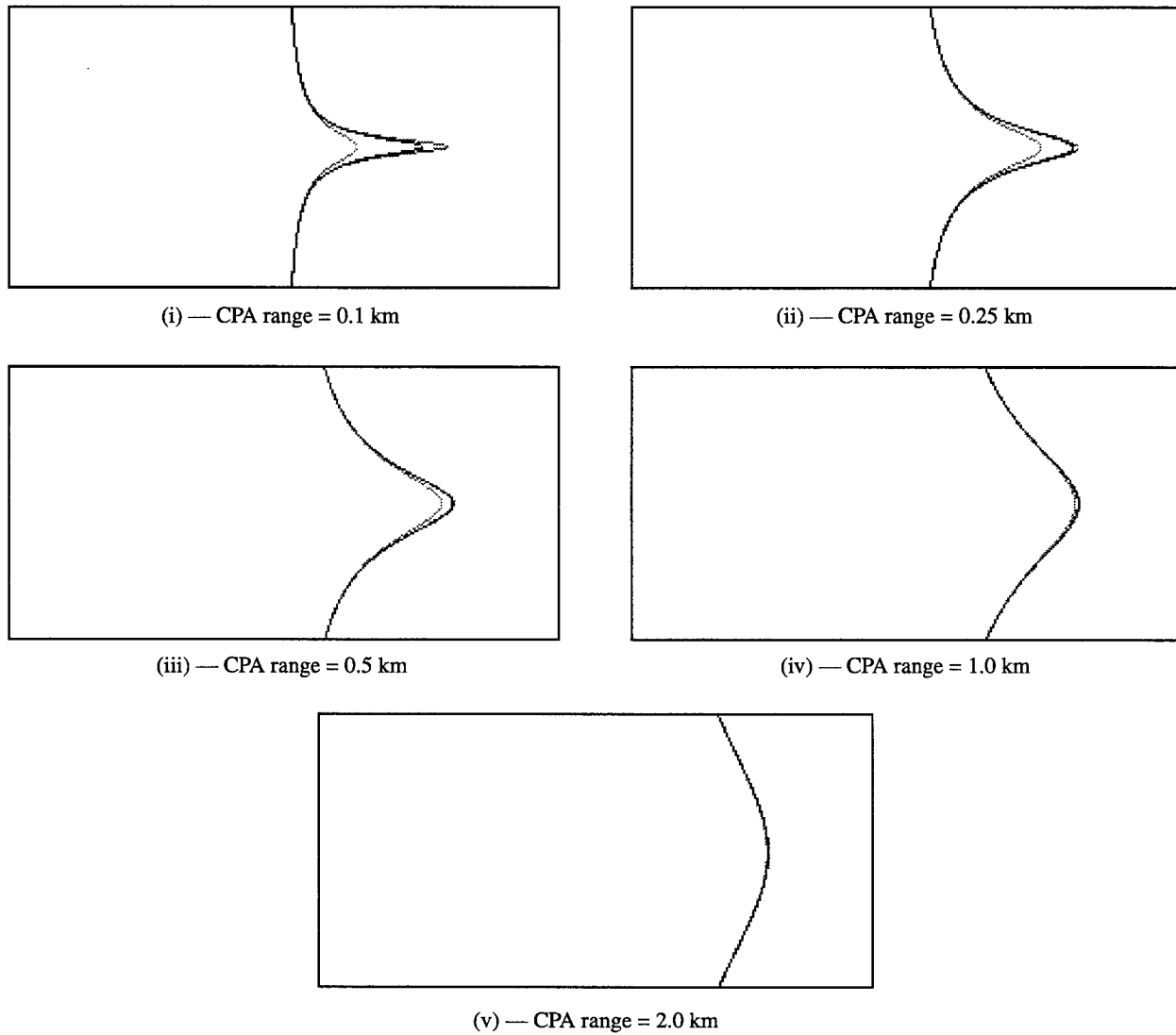
(i) — CPA range = 0.1 km

(ii) — CPA range = 0.25 km

(iii) — CPA range = 0.5 km

(iv) — CPA range = 1.0 km

(v) — CPA range = 2.0 km

Fig. 5(d) — Delay curves generated by the analytic equation using the track parameters specified in Fig. 4(d) with heading = 270°; SVP I is the lightest, SVP II is the intermediate, and SVP III is the darkest.

5. CORRELOGRAMS GENERATED WITH THE GAMARAY MODEL

For each of the SVPs, the GAMARAY model was used to produce the acoustic fields at two bottom-mounted sensors separated by 100 m for a 67 dB 10 to 150 Hz broadband signal source traveling at a speed of 4.3 knots, at a depth of 40 m, with CPA distances varying from 0.1 to 2.0 km for four target courses (0°, 30°, 60°, and 270°). The GAMARAY model included caustics and beam displacement and ignored surface scattering and the infinite paths in the caustic isonified zone. One bottom path was allowed at each bottom interaction. The acoustic fields arriving at the two sensors were then used to calculate broadband correlograms for the set parameters defined above.

Received Power as a Function of the Target Range

Figure 6 shows the received target acoustic energy as a function of the distance of the target from the sensor. The average noise level of 15 dB is shown by the horizontal dashed line. Although different SVPs produce different propagation loss, their overall behavior is consistent with the Spreading Law of transmission loss [4], and the signal power is inversely proportional to the target range. The effect due to the theoretical spreading loss on a 70 dB source $(70 - 20 \times \log(r)$, where r is the target range in yards) is shown as a thick gray line in Fig. 6.
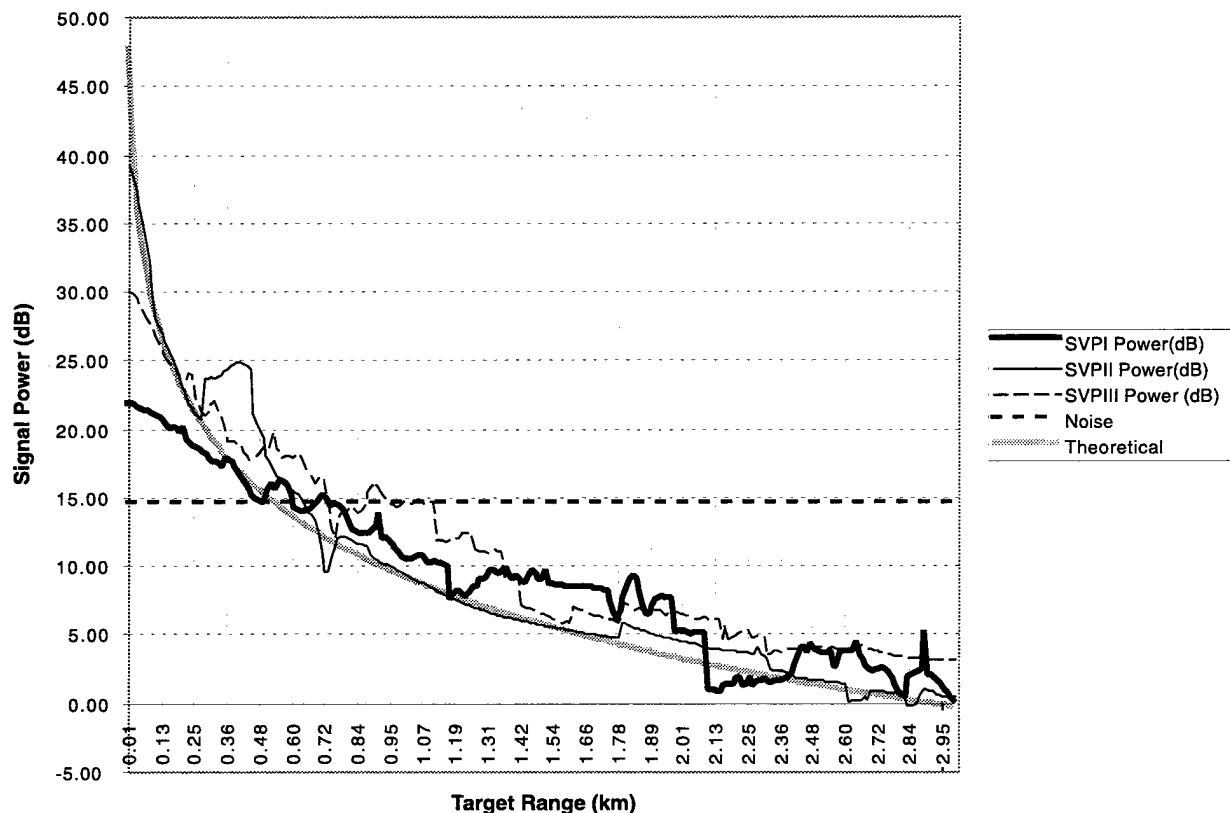

Fig. 6 — Signal power as a function of distance. The target depth is 40 m.

Eigenray Behavior as a Function of the Target Range

To study the effect of the eigenray structure on the broadband correlogram, all eigenrays within 10 dB of the strongest eigenray were tabulated. Figure 7 shows the source-receiver eigenrays for five different target ranges for the SVPs I and III. The target range varied from 0.0 to 2.5 km in increments of 0.5 km. The sensor is on the left-hand side of the figure, and the target is on the right-hand side. The sea bottom is indicated by a thick dash line, while the target positions are indicated by black dots. The dominant eigenrays are the direct path and surface reflection for short range. As the target range increases, other multipaths appear and the direct path disappears. The eigenray structure of SVP II is not shown; for the shallow depth (65 m), the water column acts as a waveguide and the dominant eigenrays are the simple direct path, the surface reflection, and the surface refraction.
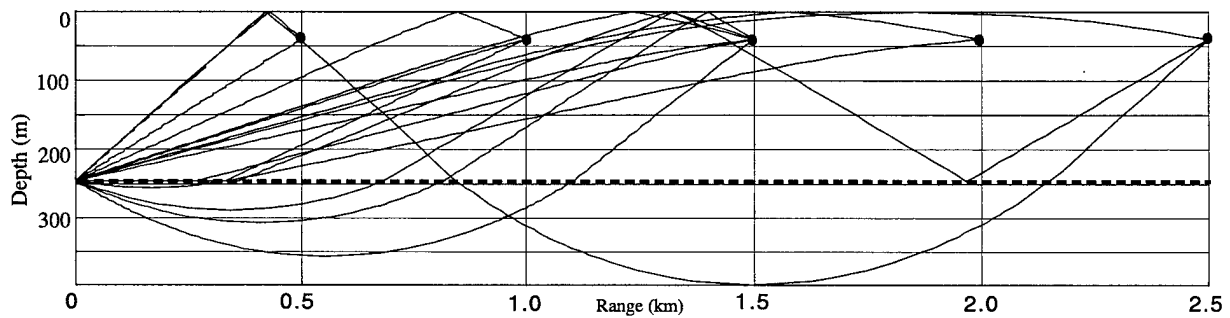

Fig. 7(a) — Dominant eigenrays for SVP I. The target is at the depth of 40 m. The depth of the water column is 245 m. The target is located at multiples of 0.5-km intervals from the sensor that is located at the left-hand side of the figure. The target positions are indicated by the black dots, and the sea bottom is indicated by the thick dash line.
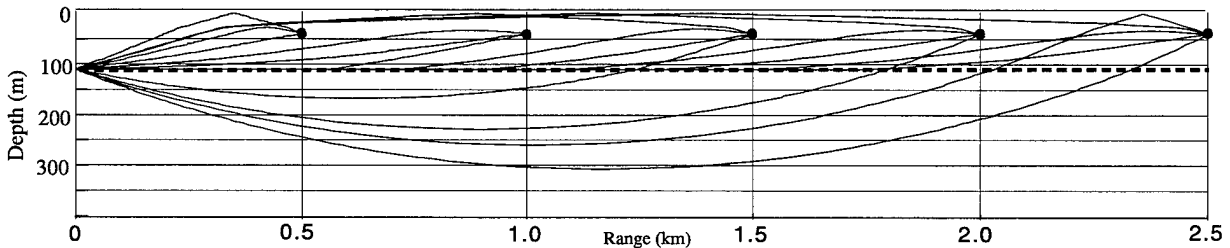

Fig. 7(b) — Dominant eigenrays for SVP III. The target is at the depth of 40 m. The depth of the water column is 110 m. The target is located at multiples of 0.5-km intervals from the sensor that is located at the left-hand side of the figure. The target positions are indicated by the black dots, and the sea bottom is indicated by the thick dash line.

For each SVP, Tables 4 through 6 provide a description of the strongest eigenrays for distances from the source to the receiver up to 3.0 km. In the tables, the initial direction, the number of surface interactions, the number of bottom interactions, the number of bottom layer traversals, and the ranges of the dominant eigenrays are shown. The ocean eigenrays are identified by a three-tuple $(d/u, \#t, \#b)$ where d/u indicates the initial ray direction as downward or upward from the signal source, $\#t$ indicates the number of surface interactions, and $\#b$ indicate the number of bottom interactions. For example, the eigenray of the direct path is identified by $(d, 0, 0)$ as the initial direction of the direct path is downward from the source and there are no surface or bottom interactions. Similarly, the surface reflection is identified by $(u, 1, 0)$ because the initial eigenray direction is upward from the signal source with one surface interaction. An asterisk (*) after d/u indicates that the interaction is a refraction, not a reflection.

Table 4 — Dominant Eigenrays for SVP I

Initial Direction	#T	#B	Bottom-Layer Traversal	Range (km)
d	0	0	0	[0.00, 2.00]
u	1	0	0	[0.00, 1.14]
d	0	1	0	[2.00, 2.34]
d	1	1	1	[2.35, 2.61]
u	2	1	1	[2.61, 2.90]
u	2	2	1	[2.90, 3.00]

Table 5 — Dominant Eigenrays for SVP II

Initial Direction	#T	#B	Bottom-Layer Traversal	Range (km)
d	0	0	0	[0.00, 0.27]
u	1	0	0	[0.00, 0.27]
u* (caustic)	1	0	0	[0.28, 3.00]

Table 6 — Dominant Eigenrays for SVP III

Initial Direction	#T	#B	Bottom-Layer Traversal	Range (km)
d	0	0	0	[0.00, 1.10]
u	1	0	0	[0.00, 0.52]
u*	1	0	0	[0.52, 1.36]
u	1	1	0	[1.36, 3.00]
d	0	1	0	[1.36, 3.00]

For SVP I, when the target is close (target range < 1.14 km[1]), only the direct path (d, 0, 0) and the surface reflection (u, 1, 0) are significant; as the target range increases, additional multipaths occur. For ranges greater than 1.14 km, the eigenray (d, 0, 1) is stronger than the surface reflection (u, 1, 0) and become the second strongest path. At 2.0 km, the direct path disappears. From 2.0 to 2.34 km, the most significant eigenray is (d, 0, 1). Propagation between target range 2.35 and 2.61 km is characterized by one eigenray (d, 1, 1). The eigenray (u, 2, 1) dominates the target ranges between 2.69 and 2.90 km, and (u, 2 , 2) dominates target ranges between 2.90 and 3.0 km.

The eigenray structure of SVP II (Table 5) is much simpler than that of SVP I. For short ranges (<0.27 km) the dominant eigenrays are the direct path (d, 0, 0) and the surface reflection (u, 1, 0). When target range is greater than 0.28 km, these paths weaken and the caustic surface refraction becomes the dominant eigenray. The direct path disappears when the target range is beyond 0.46 km.

Finally, the eigenray structure for SVP III (Table 6) is quite similar to that of SVP I. At short ranges (<0.52 km), the dominant eigenrays are the direct path (d, 0, 0) and the surface reflection (u, 1, 0). At a target range of 0.52 km, the surface refraction (u*, 1, 0) replaces the surface reflection as the second dominant eigenray. The direct path disappears beyond 1.10 km and the surface refraction (u*, 1, 0) becomes the dominant eigenray. Between 1.36 and 3.00 km, (u, 1, 1) and (d, 0, 1) are the two most significant eigenrays.

---

[1]In this section, all the range numbers are approximate. They depend on the range resolution used in the GAMARAY model.

Different SVPs can produce dramatically different propagation phenomena. For example, the direct path $(d, 0, 0)$ disappears at different target ranges (2.00 km—SVP I, 0.46 km—SVP II, and 1.10 km—SVP III). After the direct path disappears, the dominant eigenray is the caustic surface refraction $(u^*, 1, 0)$ for SVP II, $(d, 0, 1)$ for SVP I, and surface refraction $(u^*, 1, 0)$ for SVP III. Since the direct path disappears, the fundamental assumptions in the derivation of the analytic equation for the delay curve do not hold, potentially calling the DCHT method into question. However, the time difference of arrival (TDOA) of the corresponding dominant eigenrays to each sensor are very close to the TDOA of the direct path $(d, 0, 0)$ eigenrays. Thus, the correlation traces still maintain the "shape" of the correlation trace for the direct propagation, as it is the TDOA that the DCHT measures, not the actual travel times themselves.

Broadband Correlograms as a Function of the Target Range

Figures 8 through 10 show the broadband correlograms generated from the data for the three SVPs for a target traveling with a speed of 4.32 knots (8 km/h), a course of 0°, and a depth of 40 m for five different CPA values (0.1, 0.25, 0.5, 1.0, and 2.0 km). The correlation traces shown in these correlograms are identified by $p1 \times p2$ where $p1$ indicates the eigenray path arriving at the first sensor while $p2$ indicates the eigenray path arriving at the second sensor. The eigenray paths are identified by the number of water column traversals and the initial direction of the eigenray, with the initial direction immediately following the number of water column traversals. For example, the direct path will be identified as $1d$ because the direct path has only one water column traversal and its initial direction is downward, and the surface reflection will be identified as $2u$ because the surface reflection has two water column traversal, and its initial direction is upward.

The correlation traces clearly show that different SVPs affect the broadband correlogram in different ways. The most significant features are the white negative correlation traces, the width of the traces, and the fade-out of the delay curve at longer ranges. Nevertheless, the overall shape of these correlation traces is consistent with those shown in Fig 5(a).

Figure 8 shows the correlation traces for SVP I. Figure 8(a) shows three dominant correlation traces: one black and two white. The black trace, in fact, is a combination of two different correlation traces; one (identified as $1d \times 1d$) is due to the direct path, and the other (identified as $2u \times 2u$) is due to the surface reflection. The TDOA between the two direct paths ranges from 0.00245 to 0.06616 s, while the TDOA between the two surface reflection ranges from 0.00189 to 0.06503 s. Fourteen min into the run the target is about 0.19 km from the first sensor and 0.28 km from the second sensor, and the difference between the two TDOAs obtain a maximum of 0.007 s (17 pixels), which is greater than the width of the trace. As a result, two separated dark traces are seen in the correlogram. The difference between these two TDOAs gradually becomes smaller as the target moves away from this point; hence, the horizontal distance between the two black traces gradually decreases and the traces finally merge. A similar situation occurs at 17 min into the run where the target is about 0.28 km from the first sensor and 0.19 km from the second sensor. The two white traces are due to the two cross-correlations: $1d \times 2u$ and $2u \times 1d$. Since the surface reflection and the direct path are 180° out of phase, these two cross-correlation traces have negative values and appear as white traces. Because of the symmetric nature of the two, the correlation trace of $1d \times 2u$ mirrors that of the $2u \times 1d$. As target range increases, the TDOA differences between the direct path and the dominant multipath decrease. This behavior is reflected from Figs. 8(b) through 8(d). For the case shown in Fig. 8(e), the target range is between 2.0 km and 2.86 km; as explained in the previous section, the direct path disappears and the dominant eigenrays are the surface reflection, $(d, 0, 1)$, $(u, 2, 1)$, and $(u, 2, 2)$. Due to a large incoherent propagation loss, the black trace in Fig. 8(e) is barely visible. Table 7 lists the incoherent propagation losses for cases shown in Fig. 8; only the minimum and the maximum incoherent propagation loss are shown. Note the propagation loss is not uniformly decreasing. As shown in Fig. 6, there is a large drop-off for target range between 2.12 and 2.42 km.

(a) — CPA range = 0.1 km

(b) — CPA range = 0.25 km

(c) — CPA range = 0.5 km

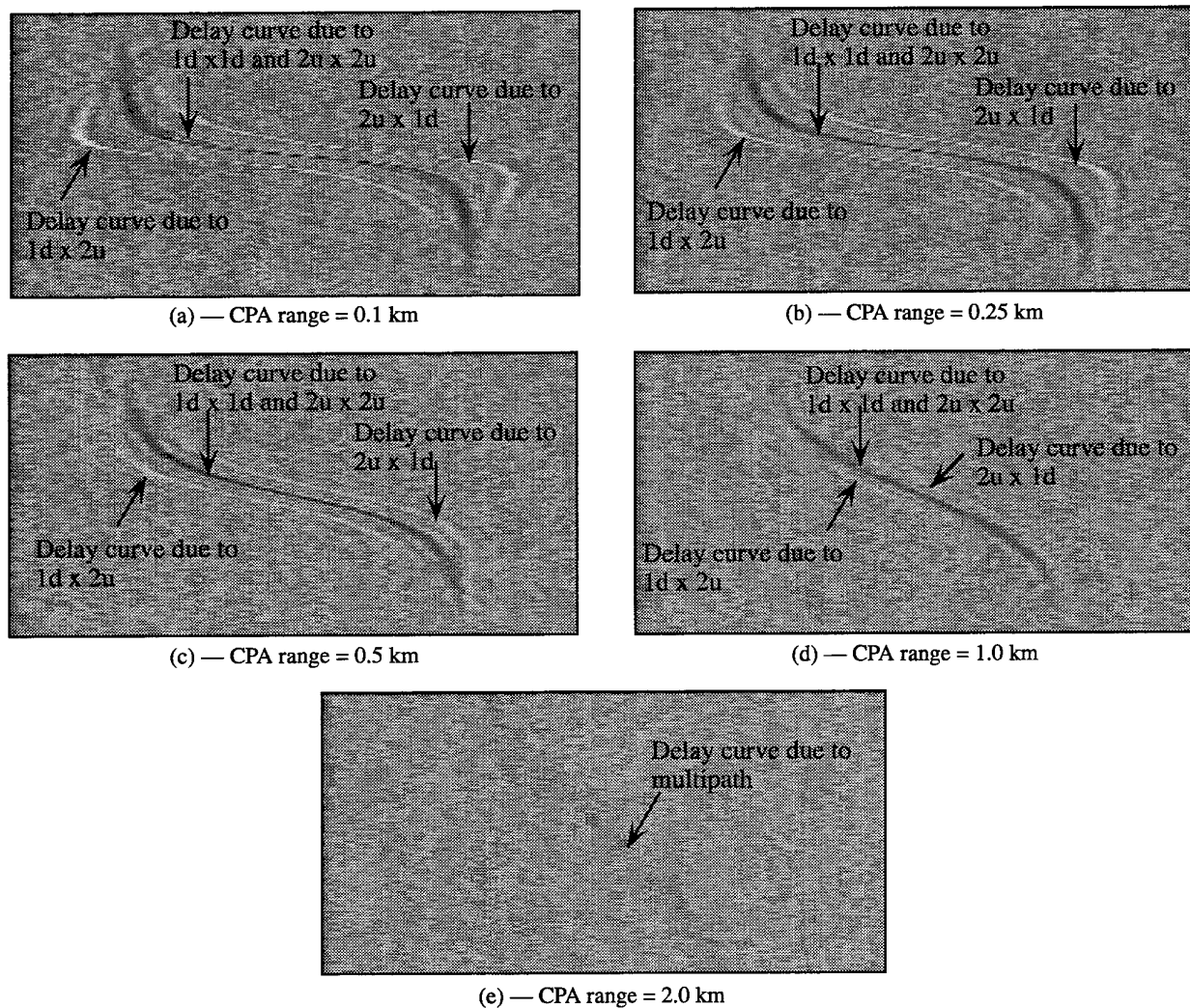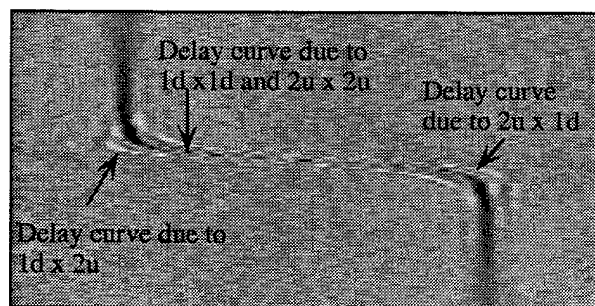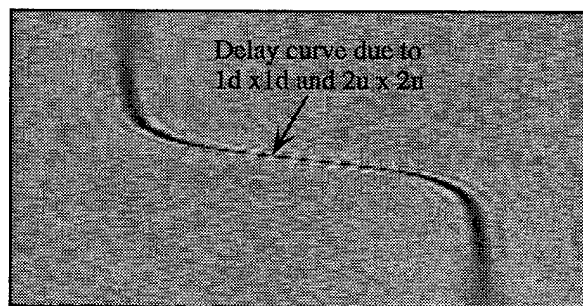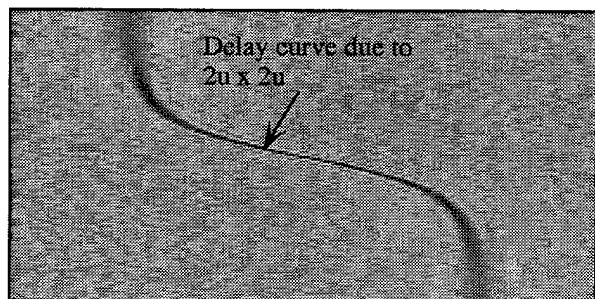(d) — CPA range = 1.0 km

(e) — CPA range = 2.0 km

Fig. 8 — Broadband correlograms from a two-hydrophone sensor system.
SVP I, heading: 0°, depth: 40 m, and speed: 4.32 knots.
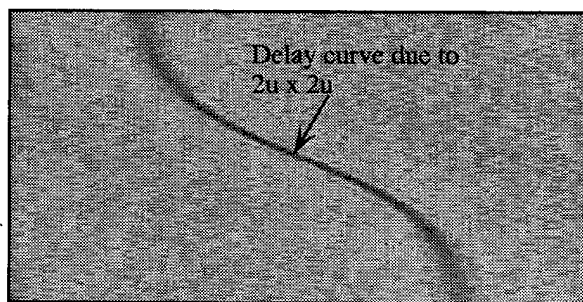
(a) — CPA range = 0.1 km

(b) — CPA range = 0.25 km

(c) — CPA range = 0.5 km

(d) — CPA range = 1.0 km

(e) — CPA range = 2.0 km

Fig. 9 — Broadband correlograms from a two-hydrophone sensor system.
SVP II, heading: 0°, depth: 40 m, and speed: 4.32 knots.

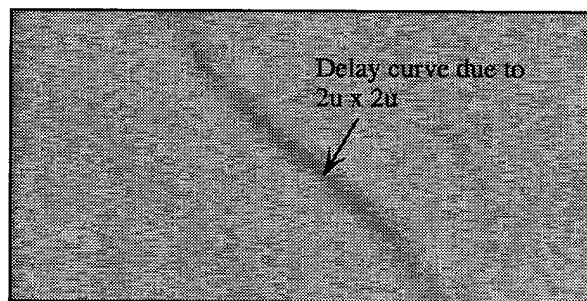(a) — CPA range = 0.1 km

(b) — CPA range = 0.25 km

(c) — CPA range = 0.5 km
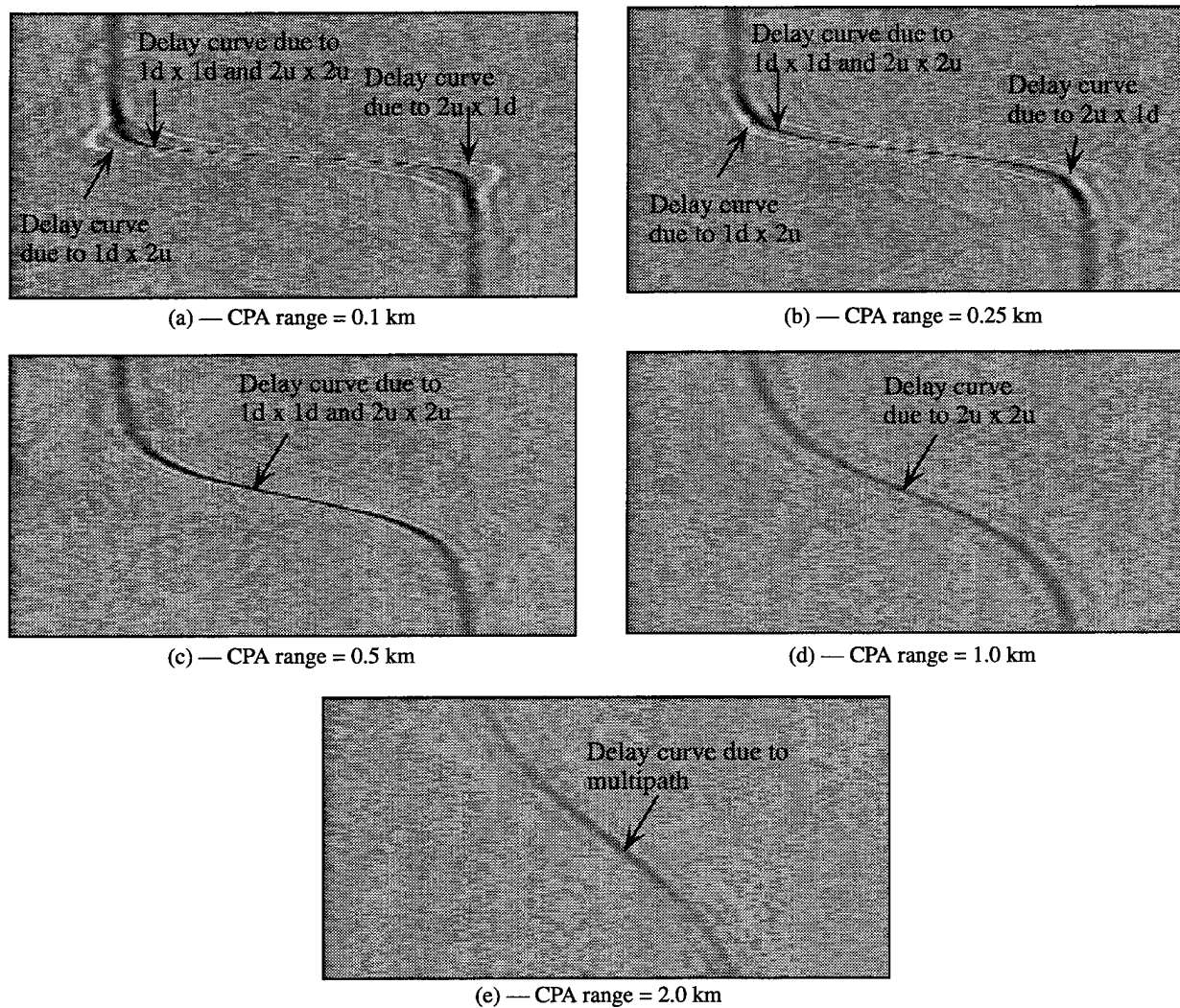

(d) — CPA range = 1.0 km

(e) — CPA range = 2.0 km

Fig. 10 — Broadband correlograms from a two-hydrophone sensor system.
SVP III, heading: 0°, depth: 40 m, and speed: 4.32 knots.

Table 7 — Incoherent Propagation Loss for Cases Shown in Fig. 8

CAP Range (km)	Min Propagation Loss (dB)	Max Propagation Loss (dB)
0.1	–45	–59
0.25	–48	–59
0.5	–52	–63
1.0	–55	–62
2.0	–61	–64

Figure 9 shows the correlation traces for SVP II for a target heading of 0°. In Fig. 9(c) through 9(e), the black correlation traces are now due to the TDOA of surface reflection since the direct path disappears in SVP II when the target range is greater than 0.5 km. The correlation trace is now observable in Fig. 9(e), although the correlation trace is wider, as the received energy is much stronger at the lower frequency band with narrower bandwidth.

Figure 10 shows the correlation traces for SVP III for a target heading of 0°. For Figs. 10(d) through 10(e), the black correlation traces are now due to the TDOA of surface reflection as the direct path disappears when the target range is greater than 1.0 km. The shape of the spectra of the received signals for SVP III is similar to those of the SVP I and, thus, the correlation traces are more visible.

Figures 11 through 19 show the correlation traces for the three different SVPs for the target heading of 30°, 60°, and 270°. The same main behaviors for SVP·I, SVP II, and SVP-III are evident, with the main difference from Figs 8 through 10 being the change in shape of the correlation trace due to target heading. This similarity is a result of the direction invariance of the propagation of the GAMARAY model.

6. DETECTION RESULTS OF DCHT

The DCHT was applied to the broadband correlograms shown in Figs. 8 through 19, using the median sound speed of each profile (1480 m/s for SVP I; 1520 m/s for SVP II; and 1520 m/s for SVP III) to compute τ_{max}. Integration was over the entire 30-min run. Table 8 shows the parameter space for the DCHT. Here, the minimum, the increment, and the maximum value for the four important parameters of the DCHT are listed. The CPA time is measured relative to the middle of the run. The searching CPA window is chosen to cover the correlogram time span. In general, the search CPA window does not need to be within the current correlogram time span; it can be extended into earlier and/or later of the current correlogram time span.

The detection results for the four target headings of the DCHT are in Tables 9 through 12. Since the value of the CPA distance (D) is known, the target speed can be estimated by multiplying v/D by D. Cells where one or more track parameters differ markedly from the real values are shaded; light shading indicates that the CPA time is incorrect, while dark shading indicates that the speed is incorrect. A negative depth value (which is meaningless) is indicated by three asterisks (***).

Although all the correlation traces are detected by the DCHT, in some cases the track parameters were incorrectly estimated. The two most significant deviations of the estimated track parameters from the correct values are the estimated target speed (twice the correct value) for SVP I when the CPA range is at 0.5 km and 2.0 km and the estimated CPA time (off about 140 s) for SVP I when CAP range is at 2.0 km. Estimates of depth were poor as only 19 of 60 were correct, and 11 of the incorrect values are physically impossible.
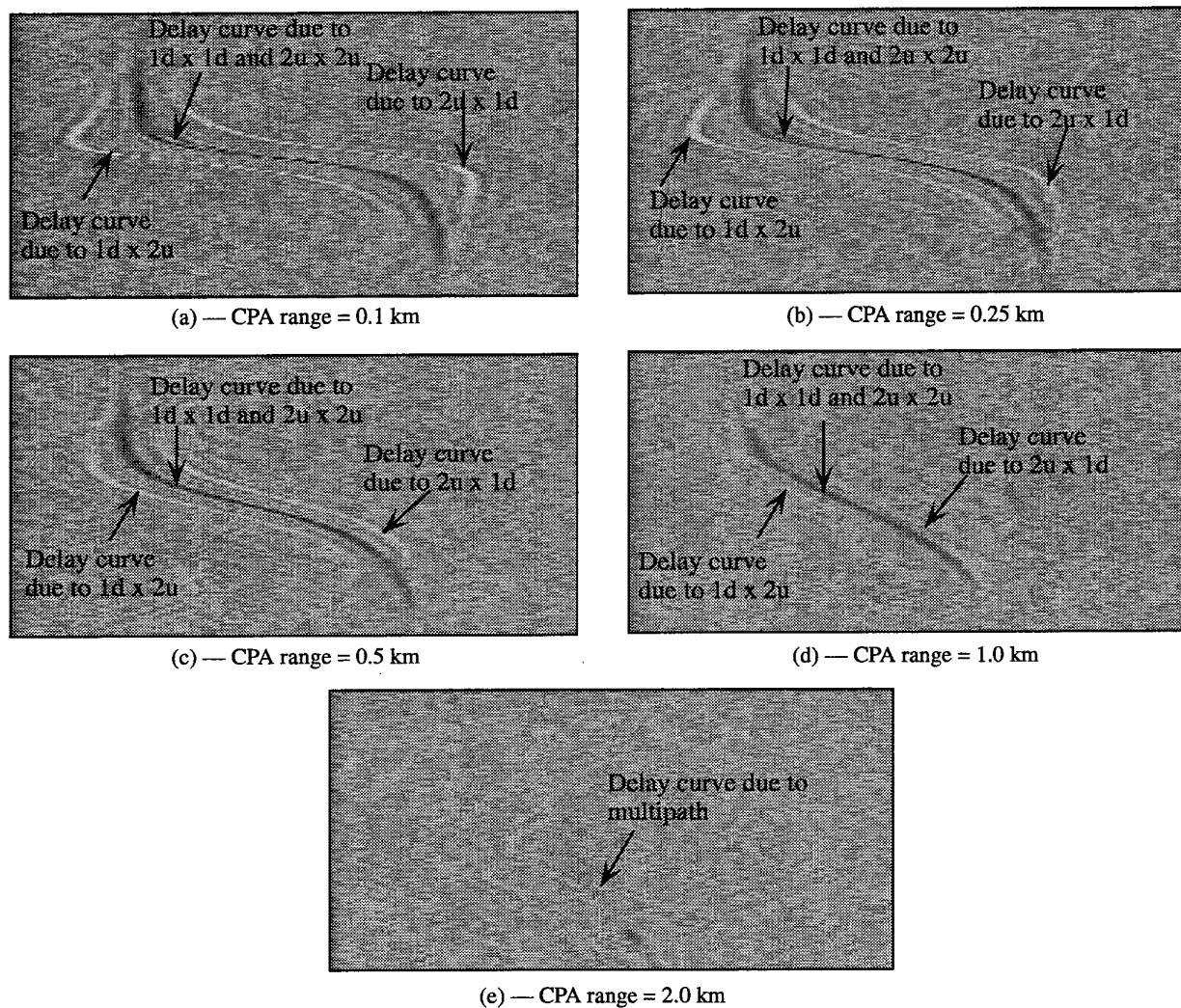
(a) — CPA range = 0.1 km

(b) — CPA range = 0.25 km

(c) — CPA range = 0.5 km

(d) — CPA range = 1.0 km

(e) — CPA range = 2.0 km

Fig. 11 — Broadband correlograms from a two-hydrophone sensor system.
SVP I, heading: 30°, depth: 40 m, and speed: 4.32 knots.

(a) — CPA range = 0.1 km

(b) — CPA range = 0.25 km

(c) — CPA range = 0.5 km
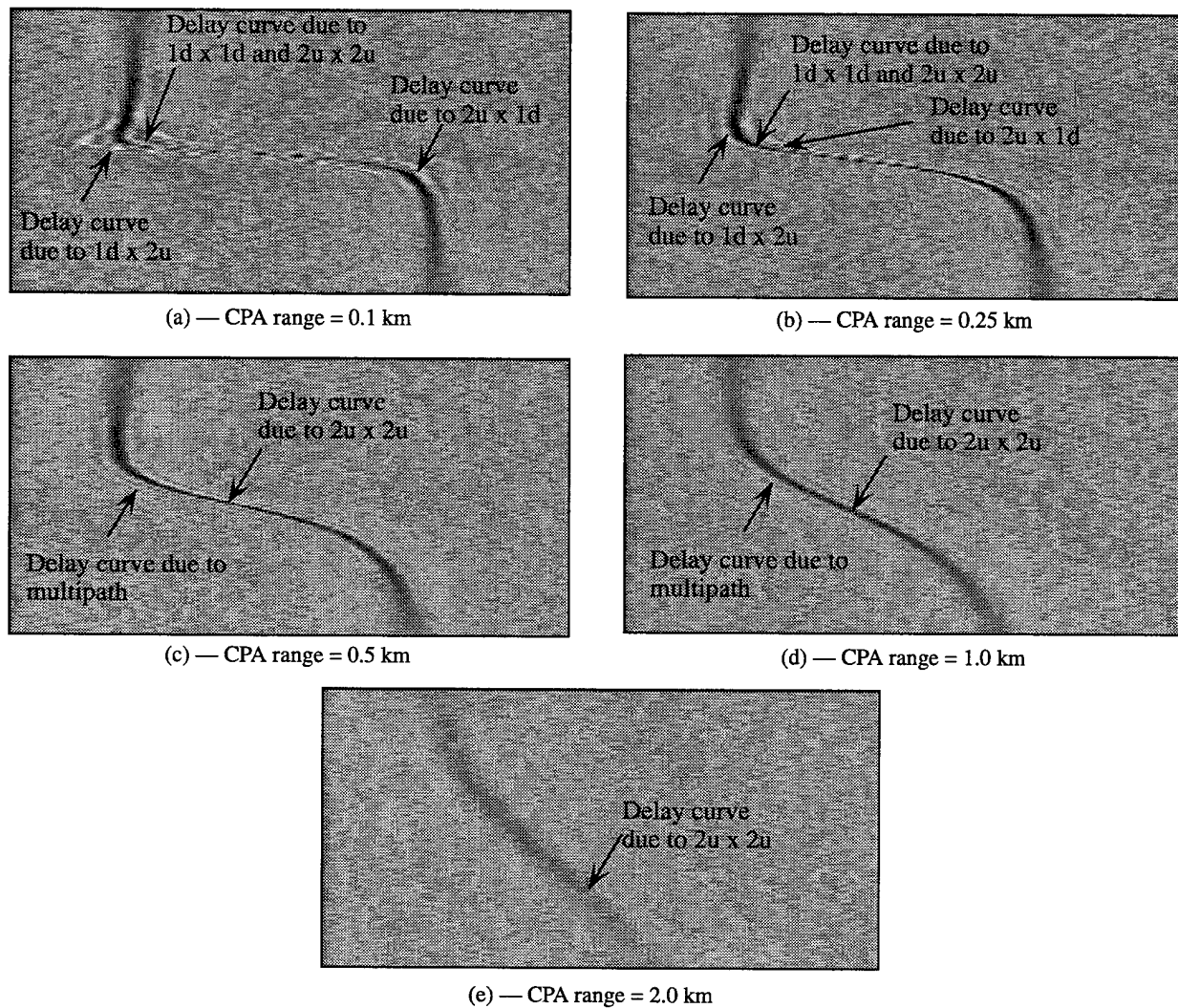

(d) — CPA range = 1.0 km

(e) — CPA range = 2.0 km

Fig. 12 — Broadband correlograms from a two-hydrophone sensor system.
SVP II, heading: 30°, depth: 40 m, and speed: 4.32 knots.

(a) — CPA range = 0.1 km

(b) — CPA range = 0.25 km

(c) — CPA range = 0.5 km

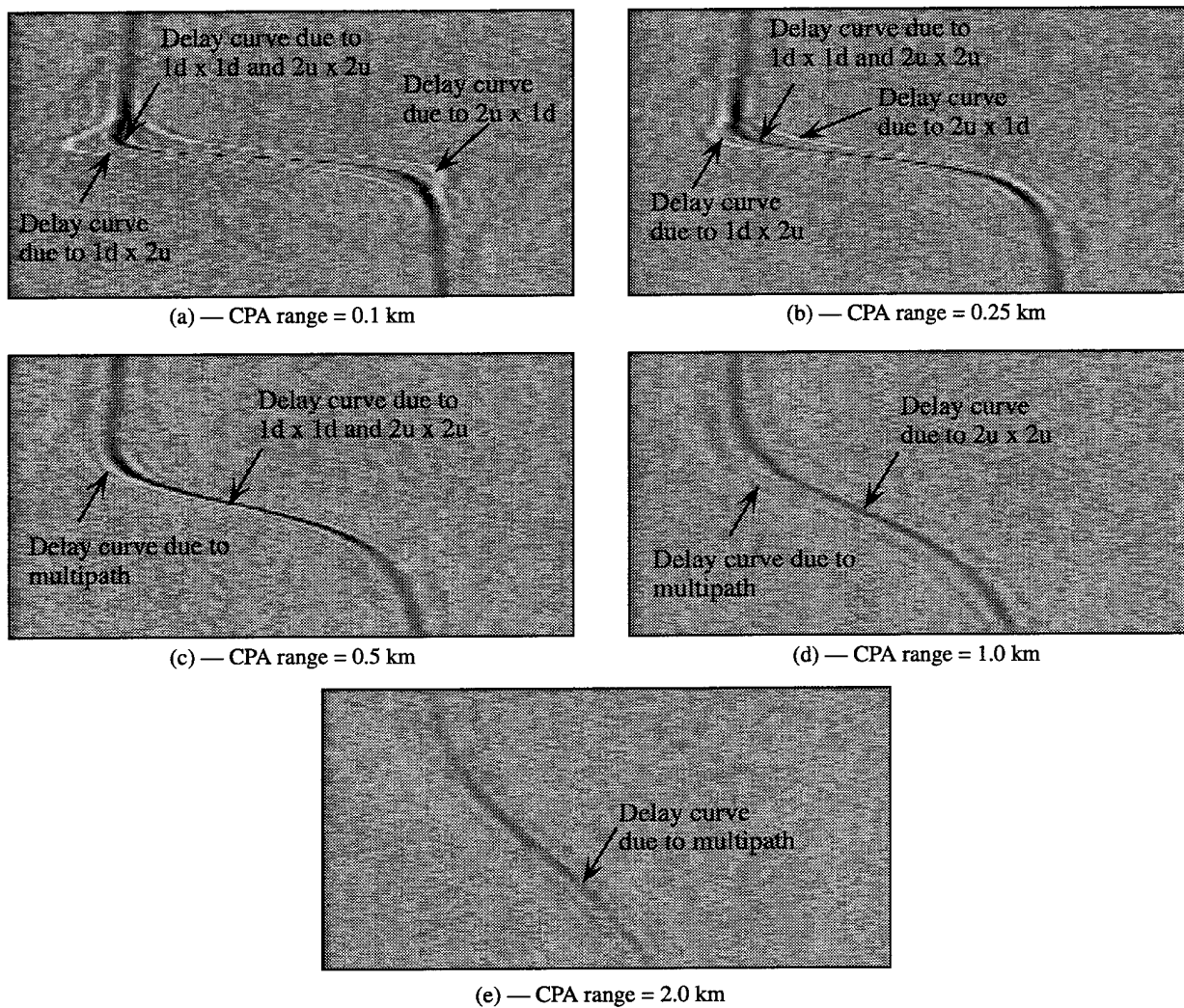(d) — CPA range = 1.0 km

(e) — CPA range = 2.0 km

Fig. 13 — Broadband correlograms from a two-hydrophone sensor system.
SVP III, heading: 30°, depth: 40 m, and speed: 4.32 knots.

(a) — CPA range = 0.1 km

(b) — CPA range = 0.25 km

(c) — CPA range = 0.5 km
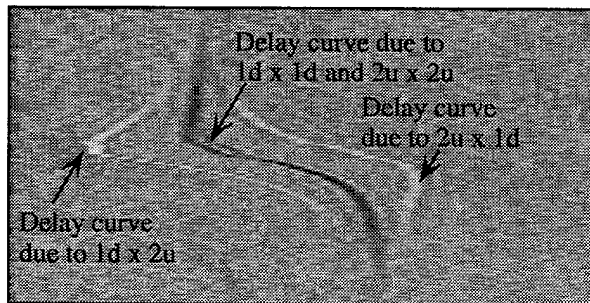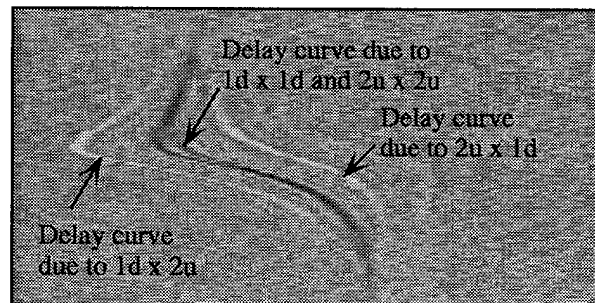

(d) — CPA range = 1.0 km

(e) — CPA range = 2.0 km

Fig. 14 — Broadband correlograms from a two-hydrophone sensor system.
SVP I, heading: 60°, depth: 40 m, and speed: 4.32 knots.

(a) — CPA range = 0.1 km

(b) — CPA range = 0.25 km

(c) — CPA range = 0.5 km

(d) — CPA range = 1.0 km

(e) — CPA range = 2.0 km

Fig. 15 — Broadband correlograms from a two-hydrophone sensor system.
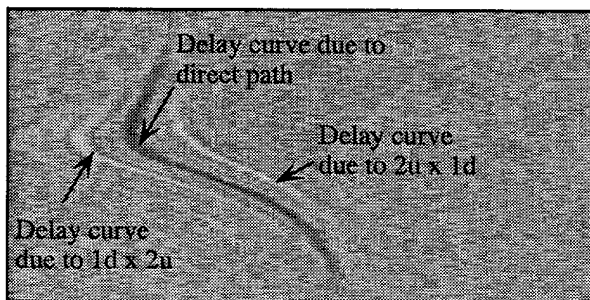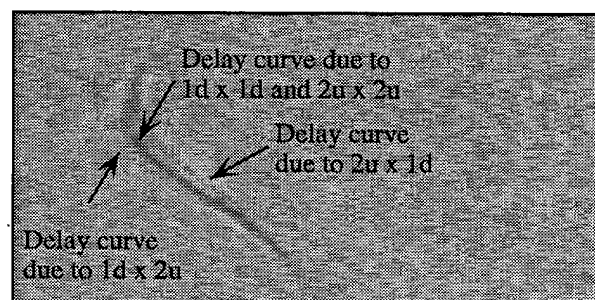SVP II, heading: 60°, depth: 40 m, and speed: 4.32 knots.

(a) — CPA range = 0.1 km

(b) — CPA range = 0.25 km

(c) — CPA range = 0.5 km

(d) — CPA range = 1.0 km

(e) — CPA range = 2.0 km

Fig. 16 — Broadband correlograms from a two-hydrophone sensor system.
SVP III, heading: 60°, depth: 40 m, and speed: 4.32 knots.
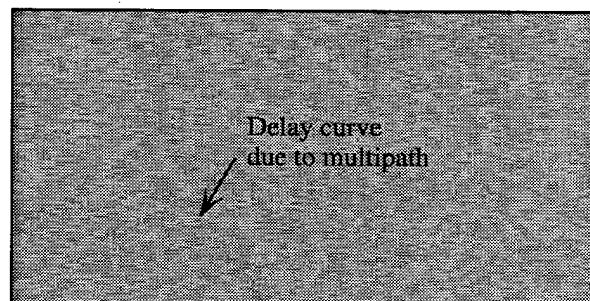
(a) — CPA range = 0.1 km

(b) — CPA range = 0.25 km

(c) — CPA range = 0.5 km

(d) — CPA range = 1.0 km

(e) — CPA range = 2.0 km

Fig. 17 — Broadband correlograms from a two-hydrophone sensor system.
SVP I, heading: 270°, depth: 40 m, and speed: 4.32 knots.

(a) — CPA range = 0.1 km

(b) — CPA range = 0.25 km

(c) — CPA range = 0.5 km

(d) — CPA range = 1.0 km

(e) — CPA range = 2.0 km

Fig. 18 — Broadband correlograms from a two-hydrophone sensor system.
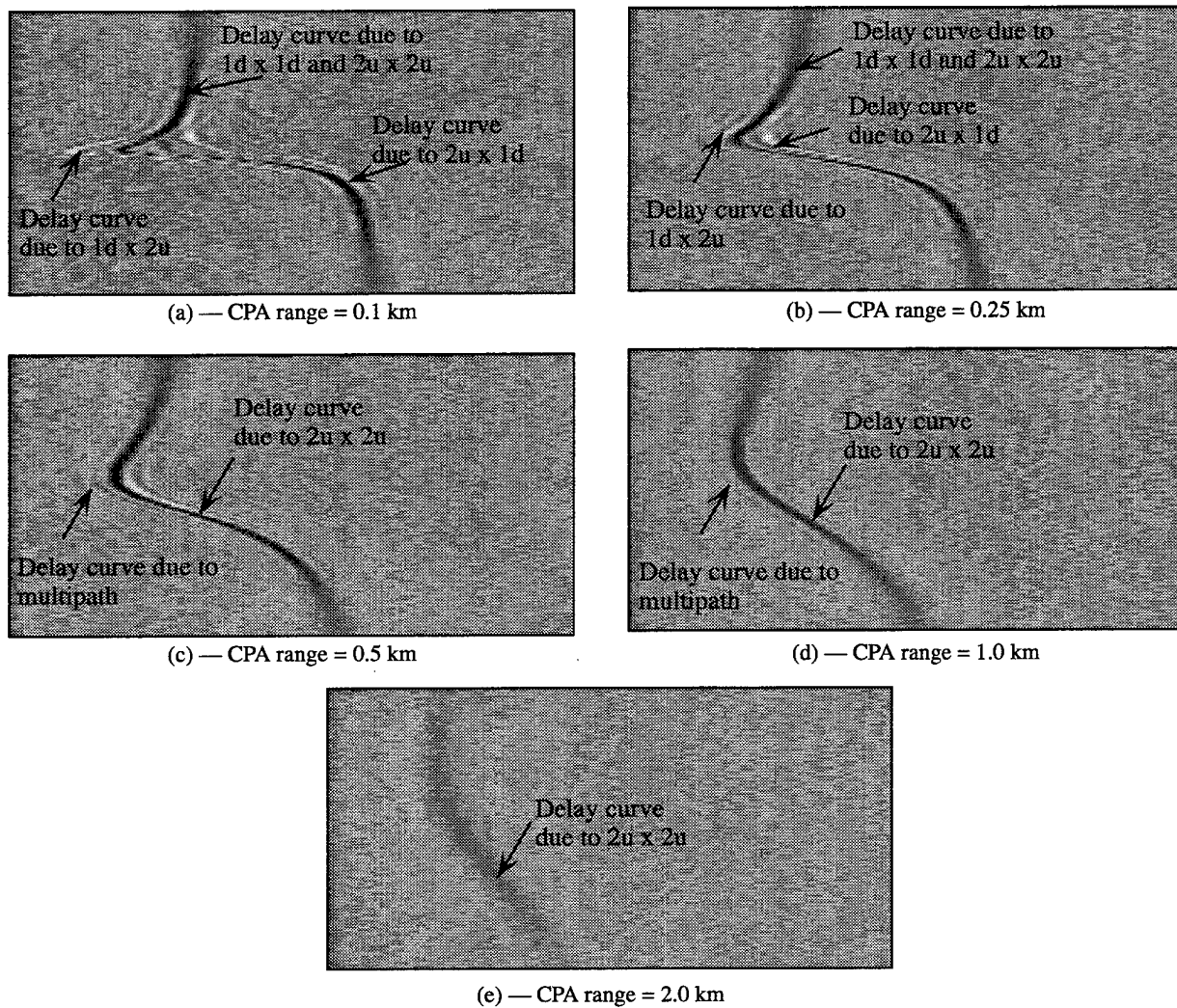SVP II, heading: 270°, depth: 40 m, and speed: 4.32 knots.

(a) — CPA range = 0.1 km

(b) — CPA range = 0.25 km

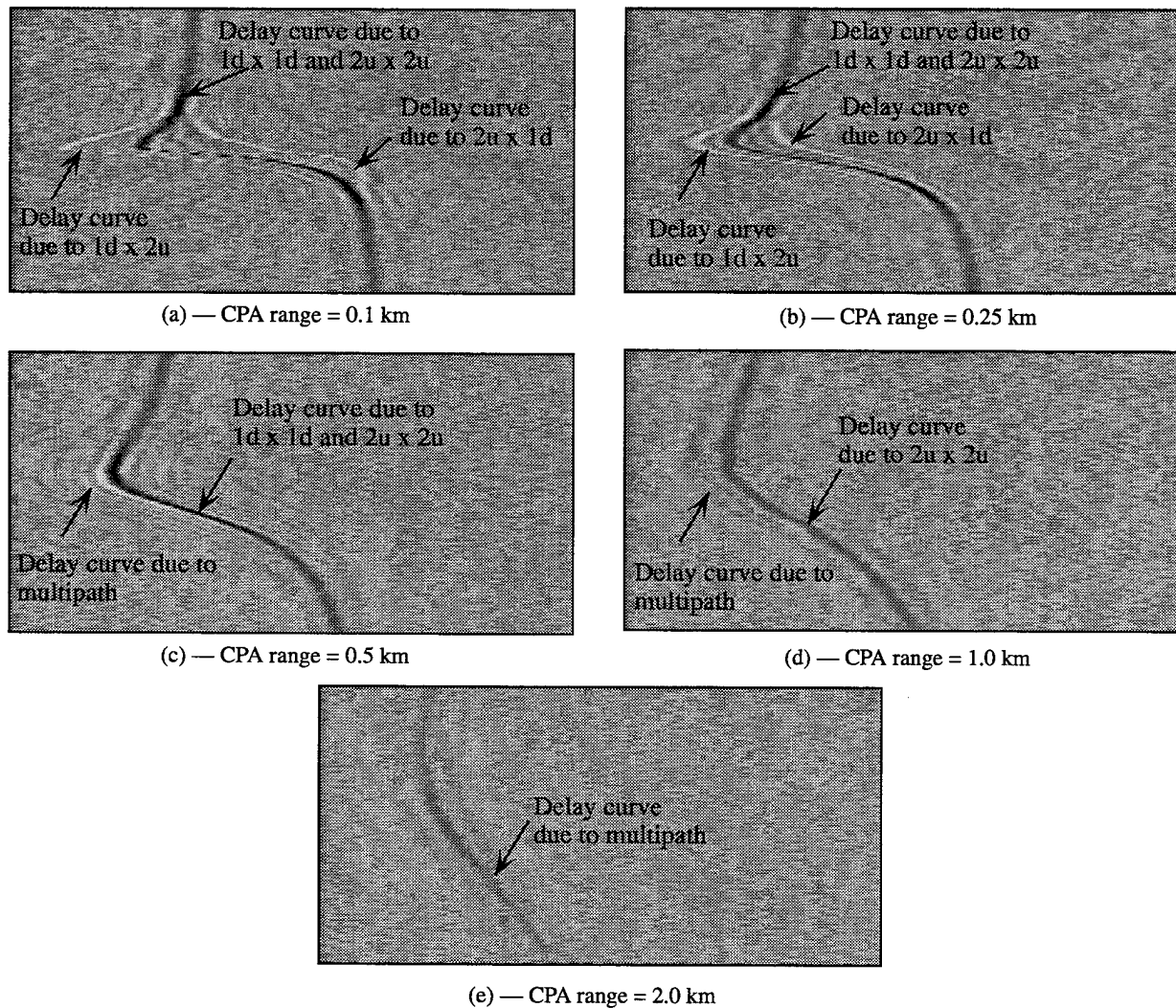(c) — CPA range = 0.5 km

(d) — CPA range = 1.0 km

(e) — CPA range = 2.0 km

Fig. 19 — Broadband correlograms from a two-hydrophone sensor system.
SVP III, heading: 270°, depth: 40 m, and speed: 4.32 knots.

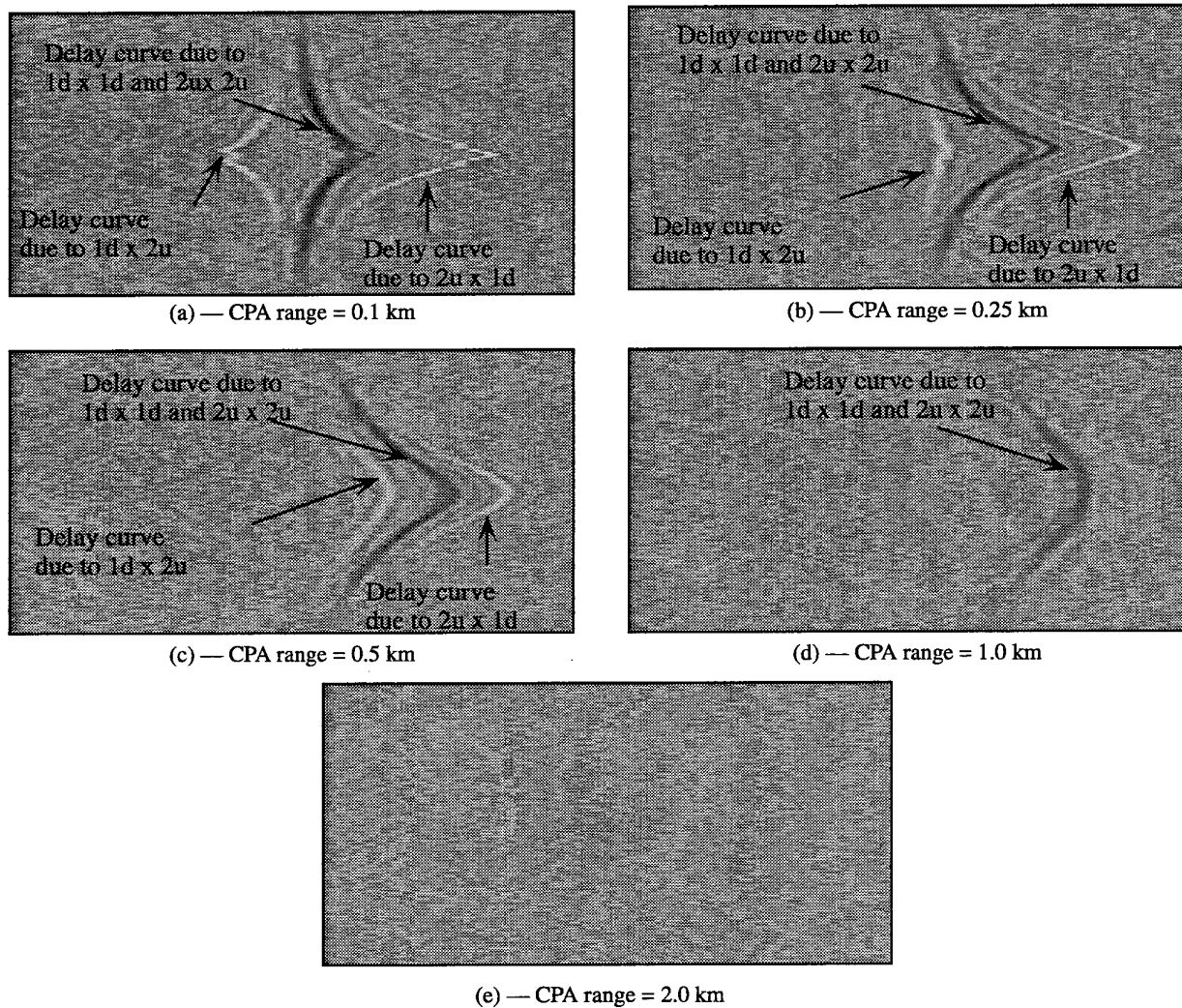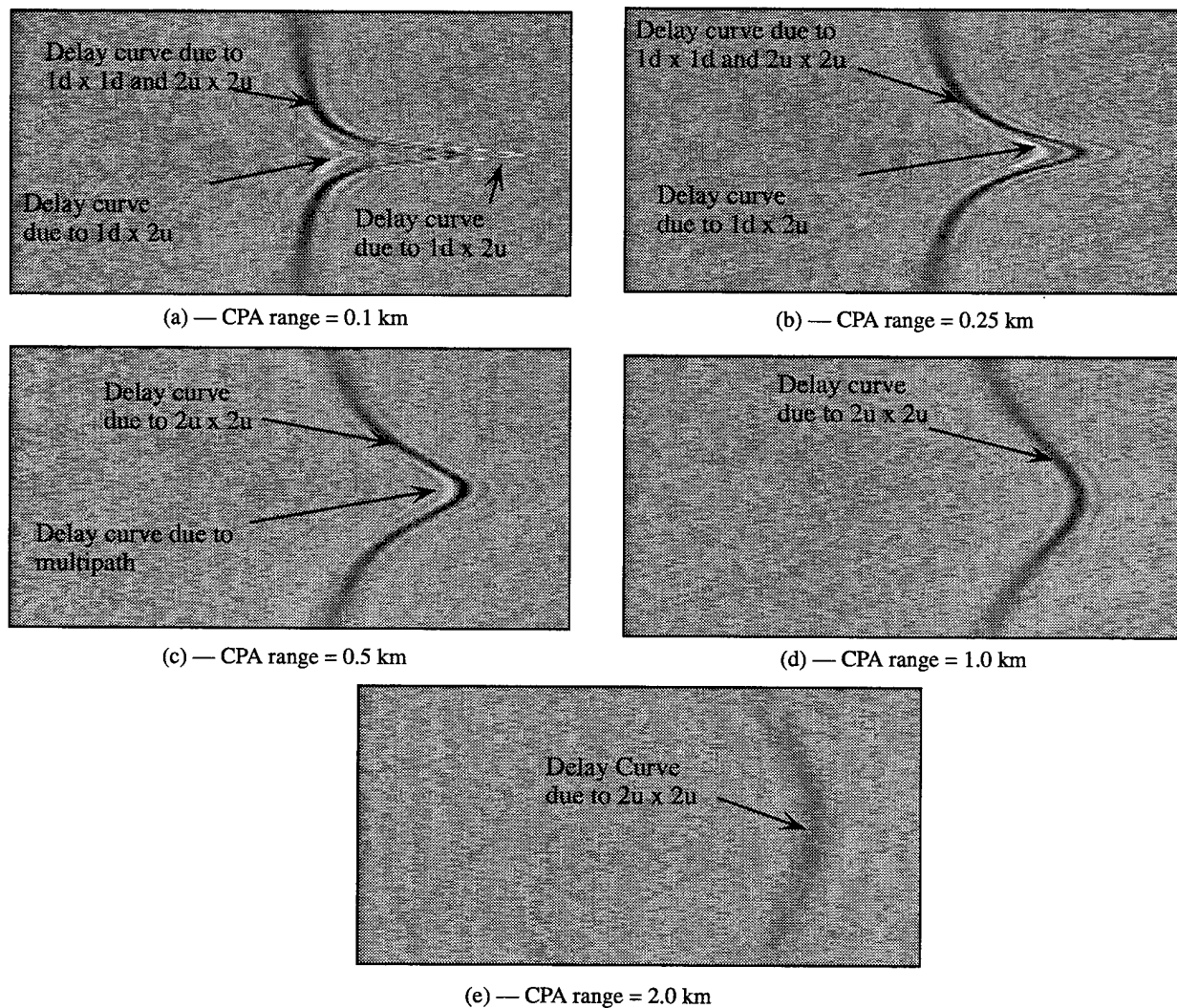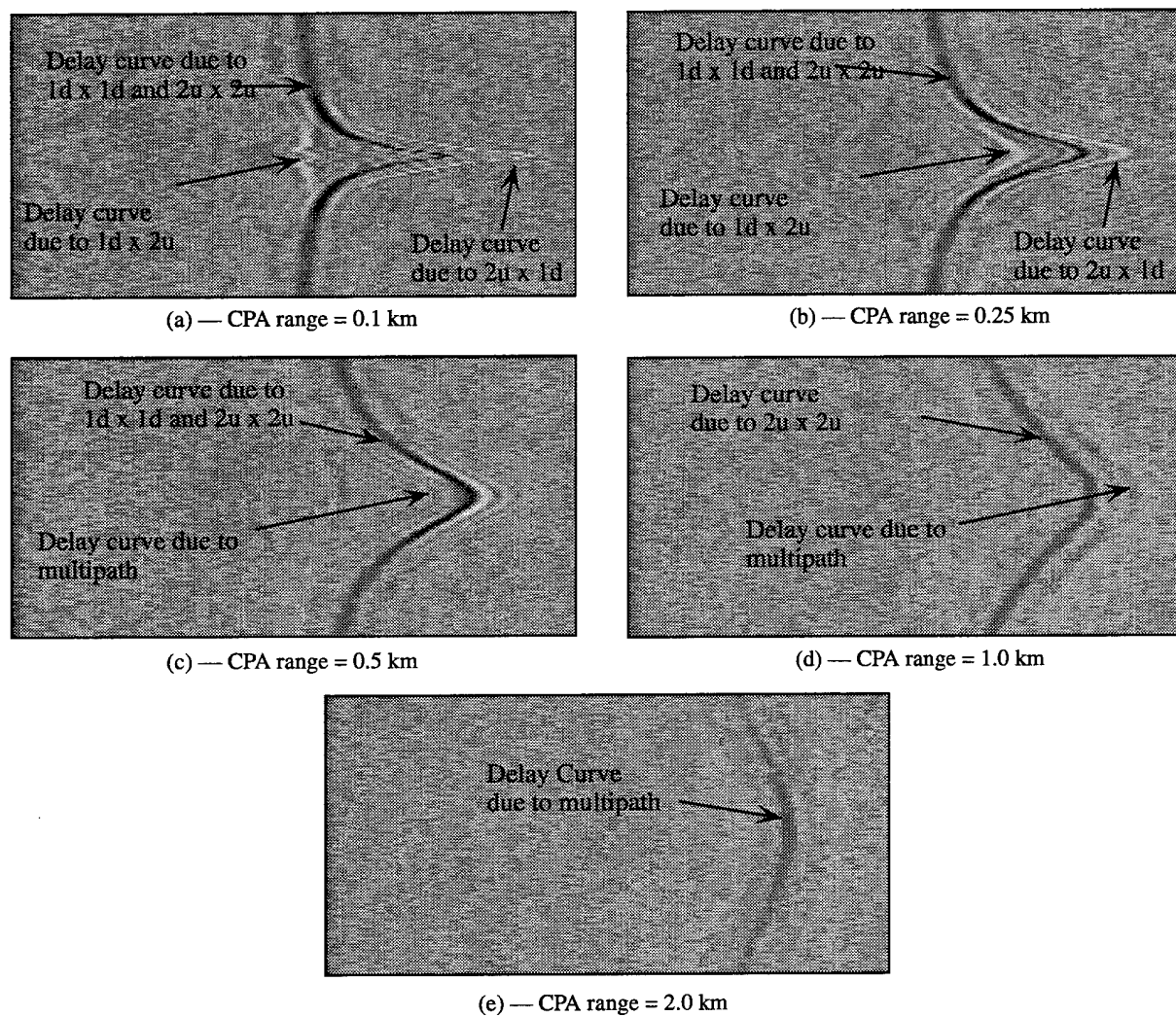Table 8 — Parameter Space Used for the DCHT

	Course	CPA Time	v/D	h/D
Min	0°	−15 (min)	0.0078	0.10275
Increment	1.41°	7 (s)	0.0082	0.10300
Max	360°	15 (min)	0.1641	2.15775

Table 9 — Results of parameter estimation by the DCHT for a target with heading of 0°, CPA time at 128th sweep, speed of 4.32 knots; depth of 40 m at different CPA ranges (0.1, 0.25, 0.5, 1.0, and 2.0 km). The track parameters are shown as a four-tuple (heading, v, t_0, h).

D (km)	Theoretical Values	Estimated Values (for SVP I)	Estimated Values (for SVP II)	Estimated Values (for SVP III)
0.1	(0°, 4.32, 128, 40)	(0°, 4.54, 129, 30)	(0°, 4.10, 129, 48)	(0°, 3.67, 129, 86)
0.25	(0°, 4.32, 128, 40)	(0°, 4.86, 129,***)	(0°, 4.32, 129, 59)	(0°, 4.32, 129, 49)
0.5	(0°, 4.32, 128, 40)	(0°, 8.64, 129,***)	(0°, 4.32, 129, 59)	(0°, 4.32, 129, 40)
1.0	(0°, 4.32, 128, 40)	(0°,4.32, 129,***)	(0°, 4.32, 129, 53)	(0°, 4.32, 129, 5.0)
2.0	(0°, 4.32, 128, 40)	(356.73°, 8.64, 134,***)	(0°, 4.32, 129,***)	(0°, 4.32, 129, 40)

Table 10 — Results of parameter estimation by the DCHT for a target with heading of 30°, CPA time at 128th sweep, speed of 4.32 knots; depth of 40 m at different CPA ranges (0.1 km, 0.25, 0.5, 1.0, and 2.0 km). The track parameters are shown as a four-tuple (heading, v, t_0, h).

D (km)	Theoretical Values	Estimated Values (for SVP I)	Estimated Values (for SVP II)	Estimated Values (for SVP III)
0.1	(30°, 4.32, 128, 40)	(31.02°, 4.32, 129, 40)	(29.61°, 4.10, 129, 39)	(29.61°, 4.10, 129, 44)
0.25	(30°, 4.32, 128, 40)	(31.02°, 4.32, 129, 40)	(29.61°, 4.32, 129, 59)	(29.61°, 4.32, 129, 66)
0.5	(30°, 4.32, 128, 40)	(31.02°, 4.32, 128, 40)	(29.61°, 4.32, 129, 59)	(29.61°, 4.32, 129, 58)
1.0	(30°, 4.32, 128, 40)	(31.02°, 4.32, 127, 40)	(29.61°, 4.32, 130,***)	(29.61°, 4.32, 130, 75)
2.0	(30°, 4.32, 128, 40)	(29.61°, 4.32, 131,***)	(29.61°, 4.32, 131,***)	(29.61°, 4.32, 131, 40)

Table 11 — Results of parameter estimation by the DCHT for a target with heading of 60°, CPA time at 128th sweep, speed of 4.32 knots; depth of 40 m at different CPA ranges (0.1, 0.25, 0.5, 1.0, and 2.0 km). The track parameters are shown as a four-tuple (heading, v, t_0, h).

D (km)	Theoretical Values	Estimated Values (for SVP I)	Estimated Values (for SVP II)	Estimated Values (for SVP III)
0.1	(60°, 4.32, 128, 40)	(60.63°, 4.32, 128, 40)	(59.22°, 4.32, 129, 39)	(59.22°, 4.32, 129, 37)
0.25	(60°, 4.32, 128, 40)	(60.63°, 4.32, 128, 66)	(59.22°, 4.32, 129, 46)	(60.63°, 4.32, 128, 93)
0.5	(60°, 4.32, 128, 40)	(60.63°, 4.32, 128, 40)	(59.22°, 4.32, 130, 34)	(60.63°, 4.32, 128, 58)
1.0	(60°, 4.32, 128, 40)	(60.63°, 4.32, 128, 40)	(60.63°, 4.32, 128, 53)	(59.22°, 4.32, 131, 75)
2.0	(60°, 4.32, 128, 40)	(54.99°, 4.32, 147,***)	(62.04°, 4.32, 125,***)	(59.22°, 4.32, 132, 40)

Table 12 — Results of parameter estimation by the DCHT for a target with heading of 270°, CPA time at 128th sweep, speed of 4.32 knots, depth of 40 m at different CPA ranges (0.1, 0.25, 0.5, 1.0, and 2.0 km). The track parameters are shown as a four-tuple (heading, v, t_0, h).

D (km)	Theoretical Values	Estimated Values (for SVP I)	Estimated Values (for SVP II)	Estimated Values (for SVP III)
0.1	(270°, 4.32, 128, 40)	(270.72°, 4.54, 127, 30)	(269.31°, 4.32, 130, 45)	(269.31°, 4.32, 130, 40)
0.25	(270°, 4.32, 128, 40)	(270.72°, 4.32, 128, 40)	(270.72°, 4.32, 128, 62)	(270.72°, 4.32, 128, 58)
0.5	(270°, 4.32, 128, 40)	(269.31°, 4.32, 130, 40)	(269.31°, 4.32, 130, 59)	(269.31°, 4.32, 130, 40)
1.0	(270°, 4.32, 128, 40)	(269.31°, 4.32, 130, 40)	(269.31°, 4.32, 130, 53)	(269.31°, 4.32, 131, 75)
2.0	(270°, 4.32, 128, 40)	(272.13°, 4.32, 121, ***)	(269.31°, 4.32, 130, 40)	(269.31°, 4.32, 131, 40)

7. THEORETICAL CONSIDERATION OF THE DEPTH EFFECT

Figure 20 shows the overlap and distortion of the delay curve due to the depth factor for target courses of 0°, 30°, 60° and 90°. When the depth factor (h/D) is small (<0.3), the delay curves of different depth factors tend to overlap each other; when the depth factor is larger, the delay curve is distorted by the depth factor, and delay curves are horizontally separated. The overlapping of the curves is highest when the target course is 0° and lowest for 90°. Overlapping of the curves for other target courses vary between these two extremes. The closer the target course is to 0°, the greater the overlapping effect; thus, it is more difficult to separate the delay curves based on depth when the target course is near 0°.

To further study the effect of h/D, the similarity measurement (the percentage of overlap) of two delay curves is examined as a function of depth. Figure 21 shows the similarity function for the four courses of 0°, 30°, 60° and 90°. The horizontal axis is the actual depth factor, while the vertical axis is the assumed depth factor. 100% similarity between the two delay curves is represented by white, and 0% similarity is represented by black. Along the diagonal, the assumed and actual depth factors are the same value so the delay curves are identical and the similarity is 100%. On the other hand, if the assumed depth factor is 1.0, while the actual depth factor is 0.0, then the delay curve generated by the assumed depth factor is very different from the delay curve generated by the actual depth factor, and the similarity between these two delay curves is just a few percent.

For small h/D, the similarity measurement is near 100%, and the delay curve can be detected even when the assumed depth factor varies from the actual depth factor. In this case, the detection of the delay curves is robust, but the estimation of the depth factor is unreliable.

Figure 21 was based on a delay curve with a width of one pixel. In the real world, delay curves have a width greater than one pixel. Figure 22 shows the similarity measurement for five-pixel-wide delay curves for the four courses of 0°, 30°, 60° and 90°. Compared with the one-pixel-wide delay curve, the bright area near $h/D = 0.0$ is enlarged and the diagonal bright area is broadened significantly. The bright areas are labeled as ambiguity area because it is difficult to determine depth factors in these areas. When the width of the delay curve is increased, the percentage of overlap between adjacent delay curves is increased accordingly. The bright area of the diagonal is widest when the target course is 0°, and narrowest when the target course is at 90°.

8. CONCLUSIONS

Shallow-water SVPs produce a complex propagation behavior with the direct path disappearing as the target moves away from the sensor. However, other eigenrays have an almost identical TDOA as that of the direct path to the two sensors, and the correlation trace preserves the shape of the delay curve. While the
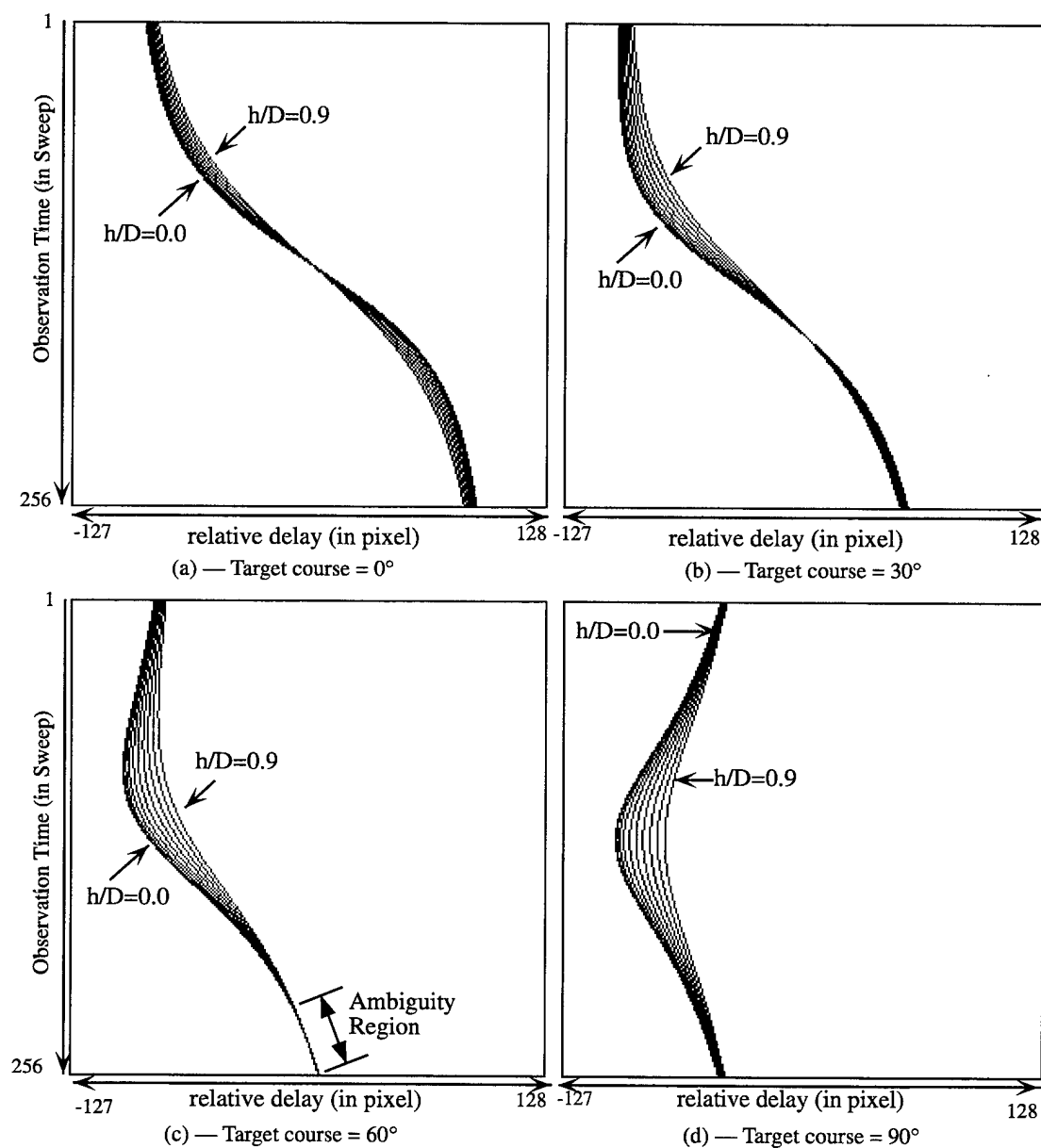
Fig. 20 — Depth effect on the distortion of delay curve. The depth factor is the ratio of the target-sensor depth difference and CPA range. There are 10 different delay curves shown in these figures. They have the same speed (3 knots), same CPA time (128th sweep), same CPA range (100 m) but with different depth factors (ranging from 0.0 to 0.9 with an increment of 0.1).
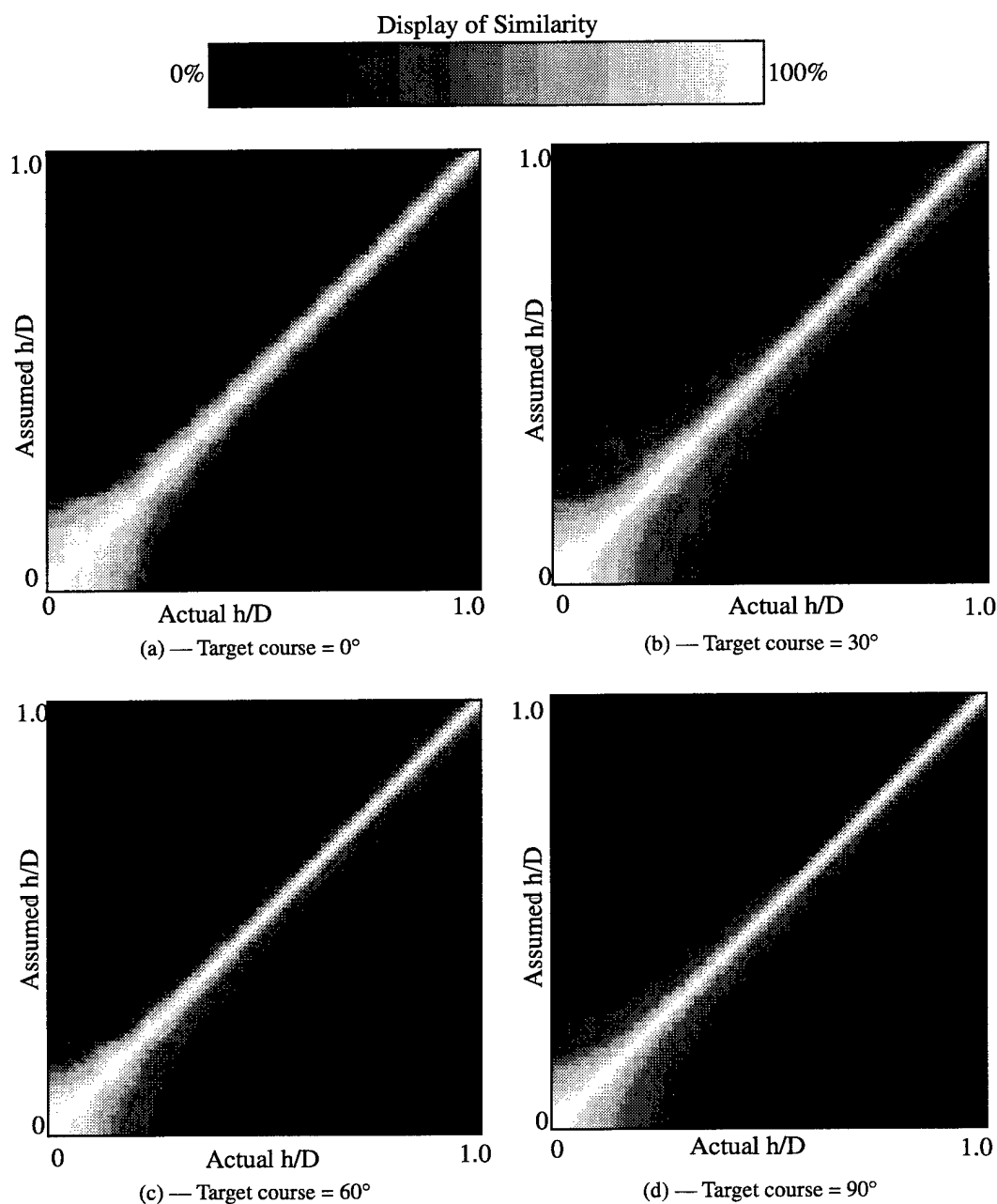
Fig. 21 — Similarity measurement for a delay curve of one-pixel wide. The horizontal axis is the actual h/D ratio of the target, while the vertical axis is the assumed h/D ratio of the target. Here h is the relative depth of the target, and D is the CPA range of the target. The target travel with constant v/D ratio (0.015432), CPA time (in the middle of the run) and course (0° in (a), 30° in (b), 60° in (c), and 90° in (d)). The length of the delay curve is 256 pixels, and the max tau is 100 pixels. Along the diagonal line, the assumed h/D has the same value as the actual h/D and, hence, will generate a perfect match, and the value of similarity is 100%. It can be observed that the similarity falls off more dramatically as the depth of the target increases.
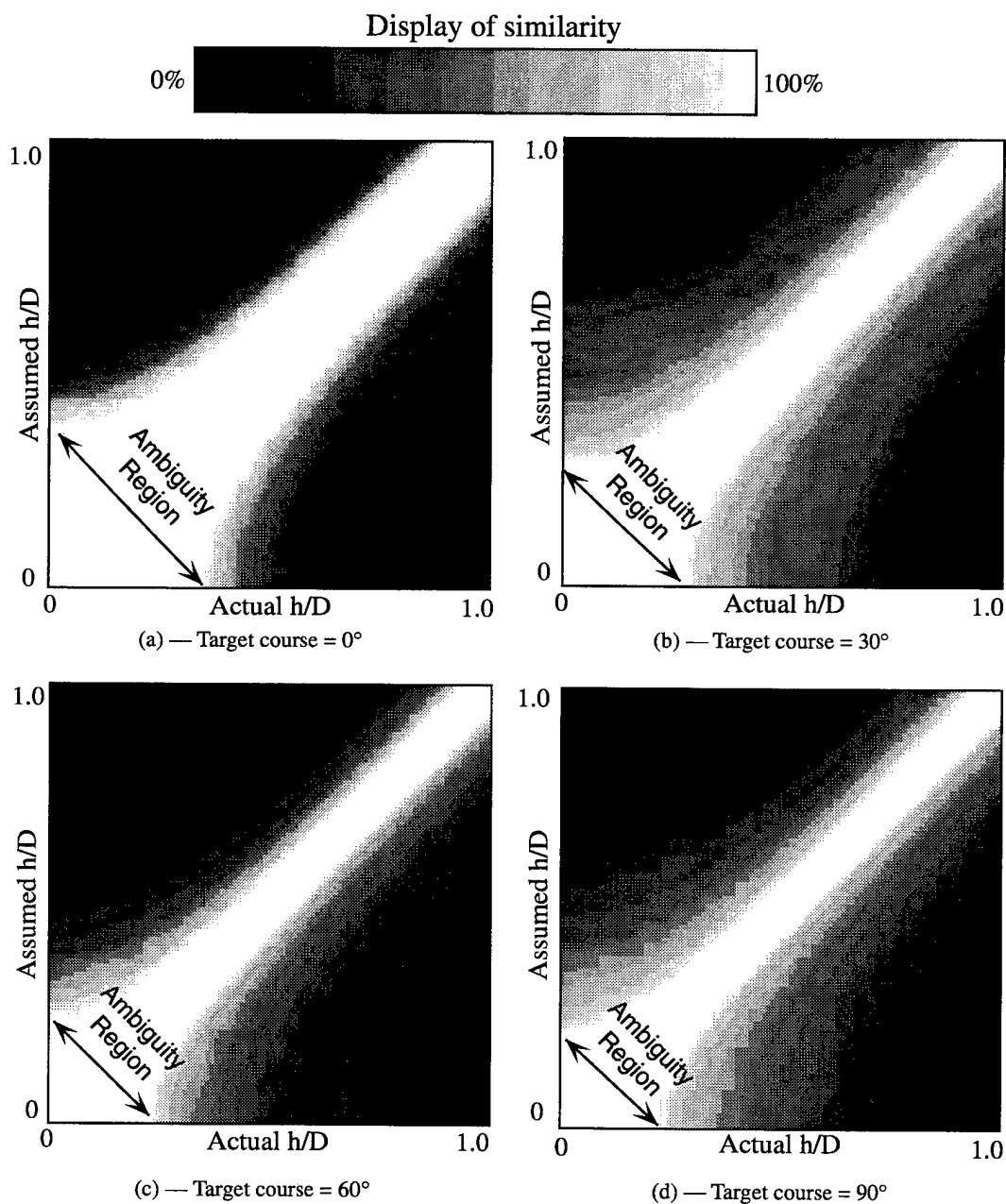
Fig. 22 — Similarity measurement for a delay curve of five-pixel wide. The horizontal axis is the actual *h/D* ratio of the target, while the vertical axis is the assumed *h/D* ratio of the target. Here *h* is the relative depth of the target, and *D* is the CPA range of the target. The target travels with constant *v/D* ratio (0.015625), CPA time (in the middle of the run) and course (0° in (a), 30° in (b), 60° in (c), and 90° in (d)). The length of the delay curve is 256 pixels, and the max tau is 100 pixels. Along the diagonal line, the assumed *h/D* has the same value as the actual *h/D* and, hence, will generate a perfect match, and the value of similarity is 100%. It can be observed that the value of the similarity falls off more dramatically as the depth of the target increases.

SVP in a shallow-water environment varies significantly over depth, a good value of the τ_{max} used in Eq. (1) for the time-delay curve can be computed by dividing the inter-sensor distance by the median value of the SVP. Based on the detection results shown in Section 6, this is a good approximation and provides good detection and parameters estimation. The DCHT remains a very useful technique for detecting the target and estimating target track parameter other than depth in a shallow-water environments, at least for the cases studied. Depth estimation from the delay curve will be most reliable when the target's course is perpendicular to the sensors' baseline and h/D is large. The detection of the delay curve will be the most robust when the target course is parallel to the sensors; baseline and h/D is small. The estimation of the depth factor should not be viewed as a precise measurement for h/D values that are small.

ACKNOWLEDGMENTS

REFERENCES

1. R. Stevens and H.-J. Shyu, "Application of the Hough Transform to Acoustic Broadband Correlograms for Passive Detection and Location," NRL/MR/5580--92-7182, January 1993.

2. E.K. Westwood, "GAMARAY User's Guide," Applied Research Laboratories, The University of Texas at Austin, Austin, Tex., October 1991.

3. F.W. Machell, "Algorithms for Broadband Processing and Display," Applied Research Laboratories Technical Report TL-EV-90-08, The University of Texas at Austin, Austin, Tex., March 1990.

4. R.J. Urick, *Principles of Underwater Sound For Engineers* (McGraw-Hill, New York, 1983), Ch. 5.

5. J.S. Bendat and A.G. Piersol, *Random Data Analysis and Measurement Procedures* (John Wiley & Sons, New York, 1986), Ch. 13.2.